Trends in Peroxyacetyl Nitrate (PAN) in the Upper Troposphere and Lower Stratosphere over Southern Asia during the summer monsoon season: Regional Impacts

S. Fadnavis[1], M. G. Schultz[2], K. Semeniuk[3], A. S. Mahajan[1], L. Pozzoli[4], S. Sonbawne[1], S. D. Ghude[1], M. Kiefer[5], and E. Eckert[5]

[1]Indian Institute of Tropical Meteorology, Pune India.
[2]Institute for Energy and Climate Research-Troposphere (IEK-8), Forschungszentrum Jülich, Jülich, Germany

[3]Department of Earth and Space Sciences and Engineering, York University, Toronto, Canada.
[4]Eurasia Institute of Earth Sciences, Istanbul Technical University, Turkey
[5]Karlsruhe Institute of Technology, Institute for Meteorology and Climate Research, Karlsruhe, Germany

Abstract

We analyze temporal trends of Peroxyacetyl Nitrate (PAN) retrievals from the Michelson Interferometer for Passive Atmospheric Sounding (MIPAS) during 2002-2011 in the altitude range 8-23 km over the Asian summer monsoon (ASM) region. The greatest enhancements of PAN mixing ratios in the upper troposphere and lower stratosphere (UTLS) are seen during the summer monsoon season from June to September. During the monsoon season, the mole fractions of PAN show statistically significant (at 2 sigma level) positive trends from 0.2 ± 0.05 to 4.6 ± 3.1 ppt /year (except between 12-14 km) which is higher than the annual mean trends of 0.1 ± 0.05 to 2.7 ± 0.8 ppt/year. These rising concentrations point to increasing NOx (= NO + NO2) and volatile organic compound (VOC) emissions from developing nations in Asia, notably India and China.

We analyze the influence of monsoon convection on the distribution of PAN in UTLS with simulations using the global chemistry-climate model ECHAM5-HAMMOZ. During the monsoon, transport into the UTLS over the Asian region primarily occurs from two convective zones, one the South China Sea and the other over the southern flank of the Himalayas.

India and China are NOx-limited regimes for ozone photochemical production, and thus we use the model to evaluate the contributions from enhanced NOx emissions to the changes in PAN, HNO_3 and O_3 concentrations in the UTLS. From a set of sensitivity experiments with emission changes in particular regions it can be concluded that Chinese emissions have a greater impact on the concentrations of these species than Indian emissions. According to SCIAMACHY NO_2 retrievals NO_X emissions increases over India have been about half of those over China between 2002 and 2011.

1. **Introduction**

The boreal summer monsoon circulation over the polluted land mass of Asia vents chemical constituents from the boundary layer into the Upper Troposphere and Lower Stratosphere (UTLS) where they are re-distributed over a wide region in subtropical latitudes (Gettelman et al., 2004; Park et al., 2004; Li et al., 2005; Randel and Park, 2006; Fu et al., 2006; Park et al., 2007; Xiong et al., 2009; Randel et al., 2010, Fadnavis et al., 2013). The chemical constituents in the UTLS influence the radiative balance and heat transport in the atmosphere (Ravishankara, 2012; Fadnavis et al., 2013). For example monsoon injection contributes ~75% of the total net upward water vapor flux in the tropics at tropopause levels (Gettelman et al., 2004). The increased amount of water vapor in the lower stratosphere could enhance ozone depletion and thus raise ultraviolet radiation levels at Earth's surface (Anderson et al., 2012). Satellite observations show convective transport and mixing of chemical constituents, (e.g. aerosols, CO, NO_X, CH_4 and HCN) in the tropical tropopause region during the Asian Summer Monsoon (ASM) season (Dodion et al., 2008; Park et al., 2009; Randel et al., 2010, Vernier et al., 2011). In the stratosphere, these chemical constituents are transported to the southern subtropics by the Brewer Dobson circulation (Park et al., 2004; Fadnavis et al., 2013) and they affect ozone, water vapour and aerosol-related constituents in the global stratosphere (Randel et al., 2010; Randel and Jensen, 2013). Peroxyacetyl nitrate (PAN) is one of such chemical species that is important in the tropical UTLS over the south Asian regions for two reasons: (1) It is a secondary pollutant with implications for the production of tropospheric ozone (O_3); (2) PAN is also a useful tracer for diagnosing transport due to monsoon convection and understand the redistribution of NO_X in the global stratosphere.

PAN mixing ratios vary from less than 1 pptv in the remote marine atmosphere (as observed in NASA GTE PEM-Tropics B campaign in the South Pacific lower marine boundary layer, data available at http://acd.ucar.edu/~emmons/DATACOMP/) to several ppbv in the polluted urban environment and biomass burning plumes (Ridley et al., 1992; Singh et al., 1998). In the UTLS mixing ratios are typically in the range 10-300 pptv (Emmons et al., 2000; Keim et al., 2008). PAN is formed exclusively from the chemical reaction of peroxyacetyl radicals ($CH_3C(O)OO$) with NO_2. The peroxyacetyl radical is generated from the oxidation of acetaldehyde (CH_3CHO) by OH, or through photolytic decomposition of acetone (CH_3COCH_3) and metylglyoxal (CH_3COCHO), which are secondary pollutants, produced by oxidation of other NMVOCs such as propene (C_3H_6). In the upper troposphere photolysis of acetone (CH_3COCH_3) is an important source of peroxyacetyl radicals (Fischer et al., 2013). The main loss reactions of PAN are thermal decomposition (most important in the lower troposphere up to ~500 hPa), photolysis (most important in the UTLS and above), and the reaction with OH. All of these reactions lead to the formation of reactive nitrogen compounds: the first two reactions yield NO_2, while the reaction with OH yields NO_3 as a product. At the surface, PAN can also be deposited. Its dry deposition velocity is on the order of 0.5 cm s^{-1} during day time and 0.1 cm s^{-1} during night time (Wu et al., 2012).

Rapid industrialization, traffic growth and urbanization in Asia cause increasing emissions of ozone precursors including NOx and VOCs. These emissions are projected to increase through 2020 in spite of the efforts of Asian countries to combat air pollution problems (Ohara et al., 2007). Most parts of Asia are NOx limited regions, i.e. controlling NOx in these regions would reduce ozone concentrations (Yamaji et al., 2006; Sinha et al., 2013). India and

China are by far the largest emitters in Asia. Satellite observations by the SCanning Imaging Absorption SpectroMeter for Atmospheric CHartographY (SCIAMACHY) and Ozone Monitoring Instrument (OMI) exhibit positive trends ~3.8 %/year in tropospheric column NO_2 over India (Ghude et al., 2013) and 7.3(±3.1) %/year over China (Schneider and van der A, 2012). Although there is a debate if these observed NOx changes can be directly related to emission changes, there is no doubt that increased NOx concentrations may enhance the formation of PAN, some of which is then transported into the UTLS by the Asian summer monsoon (ASM) circulation. In addition to PAN being transported from the polluted boundary layer it can also be formed in the upper troposphere through the production of NOx from lightning (Tie et al., 2001; Zhao et al., 2009). Lightning activity over Southern Asia is highest during the monsoon season (Ranalkar and Chaudhari, 2009; Penki and Kamra 2013). The estimated global NO_X production by lightning is ~3 Tg N/yr (Nesbitt et al., 2000; Tie et al ., 2002). Simulations with the model of ozone and related tracers (MOZART) show an increase in UTLS PAN over the ASM region due to lightning by 20-30% (Tie et al., 2001).

Thus it is interesting to examine the influence of Asian monsoon convection on the distribution of PAN in the global UTLS. Also, the impact of enhanced NO_X emissions from India and China, on the redistribution of PAN and other related chemical species, in the global UTLS merits attention. Due to the NOx limitation in India and China, the impact of enhanced VOC emissions on the distribution of PAN is expected to be smaller. Investigating this in more detail goes beyond the scope of this study, because one would have to define a credible VOC speciation and its changes over time. We employ the state-of-the-art ECHAM5-HAMMOZ chemistry climate model (Roeckner et al., 2003; Horowitz et al., 2003; Stier et al., 2005) and

perform sensitivity simulations in order to investigate the relative contributions from India and China to the increased UTLS PAN concentrations. The paper is organized as follows: Data analysis, model description and setup are described in section 2. In section 3, we discuss the distribution of PAN in the UTLS during the ASM from satellite measurements and its transport from model simulations. Section 4 contains satellite observed trends in PAN over India and China. The impact of enhanced anthropogenic Asian NO_X on PAN, HNO_3 and ozone are discussed in section 5. Conclusions are given in section 6.

2. Data and analysis

2.1 Satellite measurement

The MIPAS–E instrument onboard the ENVIronmental SATellite (ENVISAT) was launched in March 2002 into a polar orbit of 800 km altitude, with an orbital period of about 100 minutes and an orbit repeat cycle of 35 days. MIPAS–E (Fischer and Oelhaf, 1996; Fischer et al., 2008) was a Fourier Transform Spectrometer that provided continual limb emission measurements in the mid infrared over the range 685– 2410 cm−1 (14.6–4.15 μm). From June 2002 to March 2004 MIPAS operated in its full spectral resolution mode at an unapodized resolution of 0.035 cm^{-1}, and with tangent altitude steps of 3 km in the UTLS. From January 2005 through the end of the mission the spectral resolution was reduced to 0.0875 cm^{-1}, while the tangent altitude steps in the UTLS were reduced to 1.5 – 2 km. Until the platform's failure in April 2012 MIPAS monitored atmospheric minor constituents affecting atmospheric chemistry including PAN, NO_X, and O_3. The details of the general retrieval method and setup, error estimates and use of averaging kernel and visibility flag are documented by Von Clarmann et al. (2009). Details of the PAN retrievals, error budget, and vertical resolution are given by Glatthor et al. (2007) for

the 2002 – 2004 measurement period for data version V3O_PAN_5, and by Wiegele et al. (2012) for the 2005 – 2012 measurement period for data version V5R_PAN_220/V5R_PAN_221 (different naming 220/221 merely due to technical reasons). The total error of PAN retrievals is below 20% from 10-12 km, below 30% from 12-16 km, and below 40% above 16km for V3O_PAN_5 (see Fig. 2 in Glatthor et al., 2007). The error is dominated by contributions of spectral noise and the uncertainty of the instrument pointing. Table 3 in Wiegele et al. (2012) indicates that for the V5R_PAN_220/221 product the total error is below 10% from 10-12 km and above 100% for altitudes greater than 15 km. Again spectral noise and the uncertainty of the instrument pointing are the main contributors.

The sensitivity of the PAN retrievals can be judged by the averaging kernels. Since two types of retrievals are used in this study, V3O_PAN_5 and V5R_PAN_220/221 from high and reduced spectral resolution, respectively, we give two examples of the respective averaging kernel rows. The locations of the examples are 26 degree N and 81 degree E for the V3O_PAN_5 example and 28 degree N and 85 degree E for V5R_PAN_220. The figure S1 (a) and (b) shows the rows of the averaging kernels for an altitude range of 5 to 25 km. The diamonds indicate the respective nominal altitudes of the retrieval grid. The figure S1 shows that the retrieval results below 8-9 km are dominated by information from above the nominal altitude. A similar, albeit less obvious, situation develops for altitudes above 22-23 km. There and above the information has an increasing weight from lower than nominal altitudes. This is the reason why the MIPAS PAN data is not considered below 8 km and above 23 km. Another effect clearly visible in both example plots is that the altitude region which influences the retrieved PAN value at a given altitude is increasing with altitude, i.e. the vertical resolution decreases with altitude. To account

for the comparatively low, and altitude dependent, vertical resolution, the model data to be directly compared to MIPAS measurements was convolved with the MIPAS PAN averaging kernel.

In this study we analyze the MIPAS-E observed PAN data during the period 2002-2011. The data are accessible from http://share.lsdf.kit.edu/imk/asf/sat/mipas-export/Data_by_Target/. The data versions used are V3O_PAN_5 for 2002 – 2004, and V5R_PAN_220/V5R_PAN_221 for 2005 - 2011. The data is processed as per the quality specifications given in the documentation. The useful height range is specified as 5 to 23 km. The data are contoured and gridded at 8 degree longitude and 4 degree latitude resolution.

2.2 ECHAM5-HAMMOZ model simulation and experimental setup

The ECHAM5-HAMMOZ aerosol-chemistry-climate model used in the present study comprises of the general circulation model ECHAM5 (Roeckner et al., 2003), the tropospheric chemistry module, MOZ (Horowitz et al., 2003), and the aerosol module, Hamburg Aerosol Model (HAM) (Stier et al., 2005). The gas phase chemistry is based on MOZART-2 model (Horowitz et al., 2003) chemical scheme, which includes a detailed chemistry of Ox-NOx-hydrocarbons with 63 tracers and 168 reactions. The radiative transfer calculation considers the simulated concentrations of both ozone and aerosols. The $O(^1D)$, quenching reaction rates were updated according to Sander et al. (2003), and isoprene nitrates chemistry according to Fiore et al. (2005). In the MOZART chemical mechanism the PAN formation process occurs through the reaction of Peroxy Acetyl radical (CH_3CO_3) and NO_2. This reaction is reversible and the thermal decomposition of PAN back to CH_3CO_3 and NO_2 is the main sink of PAN. The reaction rates for

this reversible reaction are updated according to Sander et al. (2006). CH_3CO_3 is mainly formed by oxidation of acetaldehyde (CH_3CHO) by OH, and by the photolytic decomposition of Acetone (CH_3COCH_3) and Methylglyoxal (CH_3COCHO). In the model simulations we included emissions of acetone from anthropogenic sources and wild fires (primary sources), while acetaldehyde and methylglyoxal are produced by oxidation of other NMVOCs (secondary sources). In particular oxidation of primary NMVOCs like ethane (C_2H_6), propane (C_3H_8) and propene (C_3H_6) forms acetaldehyde, while CH_3COCHO is mainly formed from the oxidation products of isoprene and terpenes. Higher Acyl Peroxy Nitrates (MPAN) are included in MOZART-2 chemical scheme, they are also formed through oxidation of NMVOCs, but their production is not significant compared to PAN. The main loss process of PAN from the atmosphere is the thermal decomposition into its precursors. Other loss processes are photolysis and reaction with OH. In ECHAM5-HAMMOZ dry deposition follows the scheme of Ganzeveld and Lelieveld (1995). Soluble trace gases such as HNO_3 and SO_2 are also subject to wet deposition. In-cloud and below cloud scavenging follows the scheme described by Stier et al. (2005). PAN is not highly water soluble, therefore wet deposition is a minor removal process, and dry deposition is also not significant.

The model is run at a spectral resolution of T42 corresponding to about 2.8 x 2.8 degrees in the horizontal dimension and 31 vertical hybrid σ-p levels from the surface up to 10 hPa. The details of model parameterizations, emissions and validation are described by Fadnavis et al. (2013), Pozzoli et al. (2008a; 2008b; 2011). Here, we note that our base year for aerosol and trace gas emissions is 2000. Each member of our sensitivity study consists of continuous

simulations for 10 years from 1995 to 2004. Emissions were the same in each simulation, and meteorology varied because of different sea surface temperature (SST) and sea ice (SIC) data. The AMIP2 SSTs and SIC representative of the period 1995 - 2004 were specified as a lower boundary condition.

In order to understand the impact of enhanced anthropogenic NO_X emissions on the distributions of PAN, HNO_3 and ozone in the UTLS, we conducted 6 simulations for the period 1995-2004: (1) a reference experiment and five sensitivity experiments (referred to as experiments 2-6) where NOx emissions over India and China were scaled according to the observed trends. Simulation (2) increases NOx emissions over India by 38% (Ind38), run (3) those over China by 73% (Chin73). Experiment (4) shows the effect of the combined changes (India by 38%, China by 73%) (Ind38Chin73). Experiment (5) assumes equal relative changes of NOx emissions (India by 38%, China by 38% (Ind38Chin38)) in order to analyze the respective contributions, and to understand the regional emission enhancement impact on the UTLS for same emission enhancement over China. In experiment (6) emissions are increased over India by 73% (Ind73) to analyze impact of Indian emission with equal emission from China. The emission perturbations were derived from observed NO_2 trends of ~3.8% per year over India (Ghude et al., 2013) and 7.3 (±3.1) % per year over China (Schneider and van der A, 2012). Similar values of NO_2 trends (5 - 10 %/year) are also reported by Hilboll et al. (2013) over the megacities of India and China.

3. Results and discussions

3.1. Comparison with aircraft and ozonesonde measurements

Model simulated PAN, NO_X, HNO_3 and Ozone mixing ratios are evaluated with climatological datasets of airborne campaigns during the monsoon season (June-September). The data were retrieved from http://acd.ucar.edu/~emmons/DATACOMP/CAMPAIGNS/ . The NO_X and ozone volume mixing ratios observed during CAIPEEX experiment, September 2010, are evaluated over the Indian region. The details of instrument and measurement technique are available at http://www.tropmet.res.in/~caipeex/about-data.php. The list of data sets and aircraft campaigns are presented in Table 1. For the comparison, aircraft observations are averaged over 0-2 km, 2-6 km and 6-8km and at the center latitude and longitude of the flight region. Model simulations are also averaged at the same altitudes. Figure 1(a)-(k) compare the observed global distribution of PAN, ozone, HNO_3 and NO_X to those simulated by ECHAM5-HAMMOZ. The mean aircraft observations are shown as filled circles and model output are background contours. Figure 1 indicates that model simulated PAN, HNO_3 and NO_X show good agreement with aircraft measurements. Figure S2 indicates the model bias (ECHAM5-HAMMOZ-Aircraft observations) in PAN, ozone, HNO_3 and ozone. The model bias is different at each location. It varies with species and altitude. Between 0-2km, simulated PAN shows positive bias ~7-12ppt in the Western Pacific, 52-105 ppt over United States of America (USA). Ozone shows positive bias ~7ppb over India, ~3-15ppb over western Pacific, negative bias ~2-20 ppb in mid latitude Atlantic and positive bias 2-20ppb over tropical Atlantic, ~2-18 ppb over USA. HNO_3 is higher by ~20-75 ppt over Western pacific and less as ~-5 ppt at few locations. Over the UAS bias is negative less than 5 ppt. NOx shows positive bias ~40 ppt over India and 0-10 ppt over the

Western Pacific. Between 2-6m and 6-10km, over the West Pacific simulated PAN show negative bias ~10-20 ppt and positive bias ~5-50 ppt at some locations. Over the USA bias value are ~4-70 ppt. Ozone is lower by ~10-15 ppb and higher by ~3-30 ppb at some locations in the western Pacific, 3-30 ppb over Atlantic and ~2-30 ppb over USA. The positive bias in HNO_3 reduces to 3-20 ppt and negative bias to 3 to 20 ppt over the Western Pacific, over the USA negative bias is ~20 ppt and positive bias is ~3-70 ppt. The NOX shows negative bias ~40 ppt over India. The bias values vary between 6 to 10 ppt over Western Pacific, 15 to -20 ppt over USA and Atlantic. As can be seen from above discussions, ozone exhibits a low bias over South America and the Atlantic (for 0-6km). Model simulated ozone and NO_X show good agreement with CAIPEEX measurements over the Indian region. Model simulated seasonal mean ozone is compared with ozonesonde measurements (2000-2009) over three distributed stations, where vertical profiles are available for long period (1) near equator (Thiruvananthapuram: 8.4875° N, 76.9525° E, (2) tropical (Pune: 18.52° N, 73.85° E) and (3) subtropical stations (Delhi: 28.61° N, 77.23° E) over India. The simulated ozone profiles are extracted at the grid nearest to the centre of the above three stations. Figure S3 depicts that simulated ozone show fairly good agreement with ozonesonde measurements over all the three stations: In general, simulated ozone is less than ozonesonde measurements except at Delhi (between 200-100 hPa). At Delhi simulated ozone is less than ozonesonde by ~ 3-40 ppb in the troposphere and by 1000-4000 ppb in the lower stratosphere. The differences are larger at Pune (troposphere ~ 20-120ppb, stratosphere ~ 900-2500 ppb) and least at Thiruvananthapuram (troposphere ~ 10-30ppb and ~stratosphere 300-1300 ppb). This may be due to differences in spatial coverage. The ozonesonde measurements are at the stations (although ozonesonde drifts horizontally) while model simulations are at grid (2.8^{O}x2.8^{O}) nearest to the station.

3.2 Transport of PAN into the UTLS due to monsoon convection

Figure 2(a) shows the vertical distribution during the annual cycle of the MIPAS-E PAN climatology (for the period 2002-2011) averaged over the ASM region (10-40^{O}N; 60-120^{O}E). ECHAM5-HAMMOZ simulated PAN mole fractions are smoothed with the averaging kernel of MIPAS. The monthly distribution clearly shows elevated levels of PAN in the UTLS during the ASM season (June-September). Seasonal variation of ECHAM5-HAMMOZ simulated PAN (obtained from reference experiment) over this region is plotted in figure 2(b) for comparison. It also indicates plume rising into the UTLS during the ASM season, although PAN mole fractions are less than those obtained from MIPAS-E especially during July and August. These differences may be due to uncertainties in VOC, NO_X emissions, chemistry represented in the model, transport errors and model coarse resolution. Also MIPAS-E views the atmosphere from above and there are uncertainties in the MIPAS-E retrievals. The cross-section plots of (see figure S4) differences in MIPAS-E PAN with model simulated PAN indicate that in the UTLS (8-23km), MIPAS-E PAN is higher than model simulated PAN by ~20-60 ppt (except above 20km). It is lower by 20-40 ppt over eastern part of anticyclone (Southern India and South east Asia) and 20-40 ppt over Indonesia northern Australia. Near the southern pole MIPAS-E is PAN higher than ECHAM5-HAMMOZ by 20-90 ppt. The model could not produce high PAN concentrations near the southern pole between 17 and 23 km. In general, in the ASM region during the monsoon season MIPAS-E PAN is higher than model by 30-60 ppt between 8-16km and model bias vary between +40 ppt to -40 ppt between 17 to 23km. The comparison of PAN measurements from MIPAS-E with Atmospheric Chemistry Experiment-Fourier Transform Spectrometer (ACE-FTS) indicates MIPAS-E PAN is higher than ACE-FTS in the UTLS by 70 ppt at the altitudes between 9.5–17.5 km, which lies within limits of measurement error (Tereszchuk et al.,

291 2013).This indicates that model simulated PAN concentrations in the UTLS show reasonable
292 agreement with MIPAS-E.

293

294 The observed high concentrations during the monsoon season may be due to transport
295 from the lower troposphere due to strong convection and partially due to lightning activity. Thus
296 in order to study the influence of ASM circulation on the distribution of PAN in the UTLS
297 region, the seasonal mean PAN concentrations (June-September) is analyzed. We present here
298 estimates of the PAN climatology from MIPAS-E for the ASM season. Figure 2 (c) and (d)
299 exhibit the seasonal mean distribution of PAN as observed by MIPAS at 14 km and 16 km
300 respectively. PAN distribution obtained from ECHAM5-HAMMOZ reference simulations at 14
301 and 16km are plotted in figure 2(e) and (f) respectively for comparison. Figures 2(c) - 2(d) show
302 maxima in PAN concentrations (~200-250 ppt) over Asian monsoon anticyclone region (12-40N,
303 20-120E). The model is able to reproduce the maximum in PAN in the monsoon anticyclone, but
304 simulated PAN concentrations are less than MIPAS observations.

305

306 To illustrate vertical transport in the Asian monsoon region, longitude-altitude cross-
307 section averaged over monsoon anticyclone region 10-40°N and for June-September as obtained
308 from MIPAS PAN observations and ECHAM5-HAMMOZ baseline simulations (8-23km) are
309 shown in figures 3(a) and (b) respectively. Both MIPAS observations and ECHAM5-HAMMOZ
310 simulations show elevated levels of PAN (200-250ppt) over the foot hills of Himalaya (80-100E)
311 and pollution sources in Europe and Asia. The vertical winds plotted in figure 3(b) show cross
312 tropopause transport from the region 80-100^{O}E. Figure 3(c) reveals transport of boundary layer

PAN to UTLS mainly from strong convection region of the South China Sea (~100-120E) and Southern Flank of Himalaya (~80-90E). In agreement with our results, previous studies also indicate significant vertical transport due to strong monsoon convection from the southern slopes of the Himalayas (Fu et al., 2006, Fadnavis et al., 2013) and the South China Sea (Park et al., 2009). The climatology of the Advanced Very High Resolution Radiometer (AVHRR), Atmospheric Infrared Sounder (AIRS), and Moderate Resolution Imaging Spectroradiometer (MODIS) observations show frequent deep convection over the Bay of Bengal and over the foot hills of the Himalayas (Devasthale and Fueglistaler, 2010). From Trajectory analysis Chen et al. (2012) reported that the three dominant regions contributing to transport from the boundary layer to the tropical tropopause are: (i) the region between tropical Western Pacific region and South China Seas (38%), (ii) the Bay of Bengal and South Asian subcontinent (BOB, 21%), and (iii) the Tibetan Plateau including the South Slope of the Himalayas (12%).

The latitude-altitude cross section of MIPAS-E PAN concentrations (averaged over 60-120^{O}E) shows high levels of PAN over the northern subtropics (20-40^{O}N) (see figure 3(d)). The model simulated PAN shows a similar distribution (see figure 3(e)). The simulated PAN distribution at the surface reveals that the observed high levels of PAN in the UTLS are from the subtropical boundary layer (see Figure 3(f)) and are then transported upwards in deep convection. The PAN is also transported from 40-60^{O}N reaching up to 16 km. This plume is related to the biomass burning activity during this season over North-east China, Siberia, Mongolia (figures not shown). The biomass-burning emissions estimated from satellites show intense biomass burning activity over these regions during monsoon season (Choi et al., 2013).

In agreement with our results, ACE-FTS PAN measurements also shows plume (concentrations > 280pptv) rising from Siberia (Tereszchuk et al., 2013).

The boundary layer lofting of PAN by deep convection may increase NO_X and hence change the ozone concentrations in the UTLS and at remote locations to where it gets transported by the Brewer Dobson circulation (Randel et al., 2010). Another model simulation study indicates that PAN increases ozone production by removing NOx from regions of low ozone production efficiency and inject it into regions with higher ozone production efficiency, resulting in a global increase in ozone production by 2% (Walker et al., 2010). The strong lightning activity during the monsoon season (Ranalkar and. Chaudhari, 2009, Penki and Kamra, 2013) enhances the concentrations of PAN species through production of NO_X (Tie et al., 2001,2002; Labrador et al., 2005; Zhao et al., 2009; Cooper et al., 2009) that is released into a background atmosphere with some traces of VOCs. MOZART model simulations show that lightning enhances PAN emissions ~20-30% and HNO_3 ~60-80% in the middle troposphere (Tie et al., 2001). ECHAM5-HAMMOZ simulations show lightning increase in NO_X of ~ 50-70%, O_3 ~20-35%, HNO_3 ~ 50-75% and PAN ~ 20-35 over the ASM, respectively (Fadnavis et al., 2014,).

4. Trends in PAN in the UTLS of ASM region

Trends in PAN have been computed from MIPAS-E observation in the UTLS (8-23km), over the ASM region (10-40^{O}N, 60-120^{O}E), India (8- 35^{O}N, 70-94^{O}E) and China (20-45^{O}N, 85-130^{O}E). The trends are estimated with the method presented by Von Clarmann et al. (2010). To estimate vertical profiles of annual and seasonal trends we took into account altitude dependent fit parameters: 1) a possible bias between the PAN values of the 2002-2004 and 2005-2011

measurement periods (details are documented by Von Clarmann et al., 2010). 2) Amplitude and phase of the QBO, and 3) amplitudes and phases of periodic variations with periods of 3, 4, 6 and 12 months. The estimated trends are not significant at the altitudes between 8km and 9km due to the small number of data points. The trends from model simulations are calculated from difference between Ind38Chin73 and reference simulations. The estimated annual and seasonal trends are shown in figure 4(a) and (b) respectively. Model simulated and MIPAS-E observed PAN in the UTLS shows positive trends. The trends obtained from MIPAS-E observations are statistically significant at 2 Sigma level (except at few altitudes). The annual trends in MIPAS-E PAN vary between 0.1 ± 0.05 to 2.7 ± 0.8 ppt/year over the ASM region, 0.4 ± 1.3 - 3.2 ± 0.49 ppt/year over India and 1.1 ± 0.25 - 3.4 ± 1.3 ppt/year over China. Trends over India are insignificant between 12-14km. Figure 4 (a) shows that in the upper troposphere (10-14km) trends are higher over China as compared to India. In general the trend values are higher near the tropopause (~18-19km). The trends computed from model simulations are less than the trends obtained from MIPAS-E observations. This may be due to the fact that the simulations do not account for any increase in VOC emissions. However, they show similar regional variations. The model estimated trends over the ASM region vary between 0.1-1.9 ppt/year, India ~0.2-2.2 ppt/year and China ~0.8-2.4ppt/year. The increases in transportation, industrialization, and the number of coal burning power plants results in the increase of NO_X over south and eastern Asia. The satellite observed positive trends of NO_X emissions over these regions (Ghude et al., 2013; Schneider and van der A, 2012) show coherence with estimated trends in MIPAS-E PAN. The estimated trends in MIPAS-E PAN during the monsoon season are larger than annual trends at the altitude above 16 km for all the three regions. At the altitudes below 14km seasonal trends are less than annual trends.

During the monsoon season, the estimated trends are positive and statistically significant at 2 sigma level. Over India the seasonal trends in MIPAS-E PAN vary between 0.5± 0.8 and 2.7±0.47 ppt/year. In the upper troposphere, observed trends are statistically insignificant and they are negative between12-14km. The trends are higher over the China than India varying between 0.95 ± 1.2 and 2.9 ± 0.45 ppt/year, indicating that Chinese emissions contribute more to the anticyclone. The statistically insignificant positive and negative trends in the upper troposphere over India may be related to convective transport and removal of NO_X by wet scavenging in the region near southern part of Himalayas (Fadnavis et al., 2014). Model simulations for enhanced NO_X emissions over India show a non-linear increase in PAN in the upper troposphere (see the discussions in section 5.3). The variation of trends during the monsoon season computed from ECHAM5-HAMMOZ PAN is similar to the trends obtained from MIPAS-E PAN although the estimated trends are lower. They vary between ~0.9- 3ppt /year over India, ~1 – 4.5 ppt/year over China and ~0.8- 3.6 ppt/year over ASM.

Trends are larger over China than India in the upper troposphere and vice-a versa in the lower stratosphere. The 73% change in emissions over China involve larger total emissions than the 38% change over India since China emits more than India. Most of the Indian emissions are lofted to higher altitudes than the Chinese emissions by the deep convective system at the southern slopes of the Himalayas. However, a fraction of the Chinese emissions are lofted via this convective transport as well. The role of relatively shallower convective systems in lofting Chinese emissions is greater compared to India (details are given in section 5). Satellite observations show higher tropospheric NO_X concentrations over China compared to India (Schneider and van der A, 2012; Ghude et al., 2013). Because of higher absolute NOx

concentrations over China, the same percent change in emissions will lead to a larger PAN trend in this region compared to India. The amount of PAN observed in the anticyclone over the ASM region depends on the transport pathways of the air mass. During the monsoon season the air mass in the anticyclone is from polluted regions of Asia and East Asia. The polluted air (NO_X and VOCs) from these regions, transport high amount of PAN into the UTLS where temperatures are colder; hence it will retain more of PAN (Nowak et al., 2004).

The increasing trends in lightning activity during monsoon season (Penki and Kamra, 2013; Yang and Li, 2014) will increase lightning induced reactive nitrogen (NOx), and nitrogen reservoir species (HNO_3, PAN). The lightning-produced PAN is readily carried by convective updrafts to the lower stratosphere where its lifetime is considerably longer (Labrador et al., 2005). The increase in frequency of deep convective clouds over the tropical land mass (Aumann and Ruzmaikin, 2013) may cause increase in frequency of vertical transport. Radar, AVHRR, AIRS, and MODIS satellite observations show frequent overshoots deep into the tropical tropopause layer during monsoon season (Devasthale and Fueglistaler, 2010; Hassim et al., 2014). The vertical distribution of the seasonal trend suggests that there is an increasing trend in transport of PAN into the lower stratosphere due to deep monsoon convection. Thus observed increases in UTLS PAN during the monsoon season is related to increase in trends in (1) emissions at the surface, (2) frequency of overshooting convection and (3) production from lightning.

In general, the trends estimated from MIPAS-E and ECHAM5-HAMMOZ PAN larger over China than India at altitudes below 14 km and vice versa above 14 km. This may be related with the amount of pollution outflow in the upper troposphere and lower stratosphere from India and China. The pollution from China released primarily below 14 km and Chinese emissions dominate over Indian emissions. The pollution from India has substantial outflow above 14 km due to convective lifting from southern slops of the Himalayas.

5. Impact of enhanced anthropogenic Asian NO_X on PAN, HNO_3 and O_3

The satellite observations and model simulations indicate that boundary layer pollutants are lofted into the UTLS by monsoon convection (Randel et al., 2010; Fadnavis et al., 2013; Fadnavis et al., 2014). In the UTLS transport occurs through the monsoon anticyclone and across the tropopause (Fadnavis et al., 2013). The transport of boundary layer Asian NO_X into the UTLS due to monsoon convection is evident in model simulations (see Figure S5). In order to better understand the impact of enhanced anthropogenic Asian NO_X emission lifted to UTLS by ASM convection on the distribution of PAN, HNO_3, and ozone we calculate percentage change of these constituents for the Ind38, Chin73, Ind38Chin38, Ind38Chin73and Ind73 simulations with respect to reference simulations. Although we have analyzed horizontal (latitude-longitude) cross-sections at different altitudes within the UTLS (8-23km), here we present plots only at 16 km as a representative of the tropical UTLS layer.

5.1 Impact on PAN

Figures 5(a)-(e) show the percentage change in PAN at 16 km for Ind38, Chin73, Ind38Chin73, Ind38Chin38 and Ind73 simulations. The Ind38 simulation shows an increase in

PAN of ~10-18% with a 95% significance level over China and the western Pacific Ocean between Indonesia and Japan. Similar high increases also occur over the northern Caspian Sea and over Weddell Sea near Antarctica. The increase in PAN is ~1-6% over most of the other regions in middle and low latitudes. PAN decreases in polar regions reflecting a change in the diabatic circulation transport with enhanced descent of low PAN air at high latitudes in the stratosphere.

The Chin73 simulations show an increase in PAN of ~18-30% over China, and the western Pacific Ocean between Indonesia and Japan and 10-18% over India. An increase in PAN of ~20% is seen to the north of Japan and ~15% over the Black Sea, southern Pacific Ocean, southern Indian Ocean and Australia. The increase in PAN over other subpolar regions is ~1-6%. During the monsoon season, the westerly winds in the upper troposphere transport NO_y from China eastward over the Pacific Ocean. The increased values in the southern hemisphere middle latitudes similar to the maxima in the northern hemisphere middle latitudes indicate a change in the baroclinic eddy storm tracks. Since the PAN in the extratropics shown in Figure 5 is in the lowermost stratosphere it is the change in the Rossby waves penetrating from the tropospheric storm tracks that is producing the anomaly structure. This is not a long range transport feature but a reflection in a change in the circulation.

The Ind38Chin73 simulations (figure 5(c)) show increases of PAN ~14-40% over India, China and the western Pacific and ~10-20% over the Pacific Ocean (30^{O}N-35^{O}S). This gives a combined picture of Ind38 and Chin73 simulations, indicating superposing of trends. The outflow over the Pacific Ocean is more pronounced compared to the Chin73 case as is to be

expected given the Ind38 case shows transport over the western Pacific. The percentage increase of PAN in the Ind38Chin38 simulations (figure 5 (d)) shows a ~10-25% increase over India, China, and the western Pacific Ocean as in the previous cases. The pattern of PAN increase seen in the Ind38Chin38 case over central Asia and the Black Sea does not persist in the Ind38Chin73 case with non-uniform emissions increases. We attribute this to changes in the dynamics between these simulations that are induced by feedback from ozone and sulfate aerosol produced from SO_2 oxidation on the radiation. The baroclinic eddy storm track changes are not the same for the two emissions scenarios. Closer to the emissions source regions the PAN response is more linear.

Figures 6 (a)-(d) show changes of PAN in ppt. The figures for volume mixing ratio are given instead of percent since they more clearly indicate the transport pathways. There is a common pathway for PAN into the UTLS in response to increases in NOx emissions over both India and China in the strong convective uplift over the region of Nepal at the southern flanks of the Himalayas. An ensemble simulation with emissions increased by 73% instead of 38%, Ind73, (Figure 5 (e)) produced much higher values of PAN in the anticyclone region but did not produce a significant increase in the outflow over the Pacific Ocean. The increase in PAN for Ind38Chin73 simulation is 5-20% between 10-14 km and ~ 20-40% at the altitudes between 16-22 km over India and China. This is in agreement with observed trends in MIPAS-E PAN 0.5 - 2% between 10-14km and 2-4 %/year between 16-22 km. Comparison of Ind73 and Chin73 simulations show that PAN outflow over the Pacific Ocean is due to primarily to Chinese emissions with increased values over most tropical longitudes in the case of the latter. Doubling (~1.9 times) the NO_X emissions over India increases the PAN amounts by ~4 - 12% over the

ASM region and the western Pacific Ocean in the UTLS. The nonlinear response to increases in NO_X emissions over India and China is related to transport pathways. Analysis of the PAN distribution at different altitudes (not shown) indicates that emissions from India enter the UTLS over the region of Nepal but emissions from China are transported above 8 km over eastern China to the north of Vietnam. In the case of Chinese emissions, there is PAN transported over the Pacific Ocean at 8 km and at higher altitudes. The Indian emissions are being injected into the ASM anticyclone but a large part of the Chinese emissions enters the UTLS to the east of the anticyclone.

The anticyclone is an effective containment vessel for trace constituents in the UTLS around the tropopause level (Park et al., 2008). Park et al. (2009) found that emissions over India and the Bay of Bengal account for most of the CO in the anticyclone at 100 hPa and emissions over China make a secondary contribution (see their Figures 9 and 10). Convective detrainment occurs primarily below 150 hPa, which is the case over China, and only part of it becomes entrained in the anticyclonic circulation with the rest being transported to the southwest in the Hadley circulation and the northeast over the Pacific Ocean (Jiang et al., 2007; Park et al., 2009).

Another feature apparent in the 16 km distribution of PAN and the other species covered in this section is that the overall change is positive in the tropics and negative in the extratropics. This indicates an intensification of the Brewer-Dobson circulation since there is no chemical mechanism to explain this pattern for all these species. Changes in the synoptic scale circulation

515 are also evident in the positive and negative tracer anomaly structures in the extratropics. At 16
516 km this reflects Rossby wave changes induced by shifting of the baroclinic eddy storm tracks in
517 the troposphere associated with the nonlinear dynamical response to heating perturbations in
518 response to chemical changes.

519

520 **5.2 Impact on HNO_3**

521 Changes in distribution of HNO_3 (%) at 16 km due to enhanced anthropogenic Asian NO_X
522 emissions are shown in figures 7(a)-(e). Ind38 simulations show 1-5% increase in HNO_3 over
523 most of the regions with a 95% statistically significant high of 10-14% over the South China Sea
524 and a high of over 20-25% over the East China Sea. The Chin73 simulations show increase in
525 HNO_3 in a region between 30S and 30N with few patches over other regions. There is a
526 significant increase in HNO_3 ~14-40% over the monsoon anticyclone and over 30% over South
527 East Asia, China, South and East China Seas and over the western Pacific Ocean south of Japan.
528 There is an increase (95% confidence level) in HNO_3 of ~8-14% over the tropical Pacific Ocean
529 extending to South America. The Ind38Chin73 and Ind38Chin38 simulations show statistically
530 significant increases of HNO_3 in the monsoon anticyclone region. However, comparing the India
531 and China uniform and non-uniform emissions increase cases it is apparent that a 38% increase
532 in NOx emissions over China is not sufficient to drive a significant HNO_3 response over the
533 central and eastern Pacific Ocean. The dynamical response to the NOx emissions changes is such
534 that HNO_3 is lower in most of the extratropics at 16 km.

535

536

5.3 Impact on NO_y

In this section we present impact of enhanced NOx emissions on NO_y. The NO_y is computed from

$NO_y = NO+NO_2+NO_3+2*N_2O_5+HNO_3+HNO_4+PAN+MPAN+ONIT+ONITR+ISOPNO_3$.

The impact of enhanced NO_X emission over India and China (Figure 8 (a)-(e)) lead to changes in NO_y (in the UTLS) similar to PAN and HNO_3 (see Figures 5 and 7). The increase in NOx emissions over the Indian region lead to an increase of high amount of NO_y over China (1-11%) and the western Pacific Ocean (2-11%) while increase in NO_X emissions over China increases NO_y over India (2-15%), South East Asia (3-11%) and South China Sea (7-15%), Indian Ocean (3-15%)and Pacific Ocean (2-15%).

Figures 5-8 show that increase in NO_X emissions over India, increases PAN, HNO_3 and NO_y in the UTLS over South East Asia and South China Sea. Concentration of these species is less over the Indian region especially near southern parts of the Himalaya, from where boundary layer Indian pollutants are transported into the monsoon anticyclone (Fadnavis et al., 2013). However, increase in NO_X emissions over China increases PAN, HNO_3 and NO_y into the monsoon anticyclone. Part of these emissions is taken up by the westerly winds and is transported over the Pacific Ocean. Similar increase in PAN, HNO_3 and NO_y is also observed for Ind38Chin38 and Ind38Chin73 simulations. The low concentration of HNO_3, PAN and NO_y over the convection region of the Himalaya may be due to removal of NO_X by wet scavenging. The ozone distribution at 860 hPa show (figure not shown) for Ind38 simulations show high anomalies over India and making its way over the Pacific Ocean to North America. The

559 longitudinal transect of HNO_3 (see figure 7 (f)) indicates that HNO_3 is depleted around 100
560 degrees East and this removal process is less effective going farther to the east, i.e. over China
561 and South-East Asia. It is possible that the extra NOx over India is being locked up as HNO_3 and
562 removed by wet scavenging. High amount of water vapour present in the atmosphere during the
563 monsoon season, may remove NO_X by the reactions: $NO_2+OH \rightarrow HNO_3$ and $N_2O_5 + 2\ H_2O$
564 $\rightarrow 2HNO_3$ that yields HNO_3 is more active in the convective zone south of the Himalayas. So the
565 efficiency of NOx conversion to HNO_3 is larger compared to that over China. A number of
566 previous studies (Holland and Lamarque, 1997; Shepon et al., 2007) have reported that wet
567 deposition of HNO_3 is the most important pathway of NOx removal in the free troposphere. The
568 ECHAM5-HAMMOZ analysis of convective heating and vertical ascent in the troposphere over
569 the region of Nepal is more intense than convective systems over China. This indicates that
570 HNO_3 differences are not only due to transport but may reflect differences in wet deposition as
571 well.
572
573 **5.4 Impact on Ozone**
574 Changes in ozone at 16 km due to enhanced Asian anthropogenic NO_X are shown in
575 figure 9(a) - (e). Increase in NO_X emissions over India (Ind38), increases ozone (3-7% or 20-60
576 ppt) over the Indian Ocean and South China Sea. Chin73, Ind38Chin38, Ind38Chin73
577 simulations show increase in ozone (3-10% or 20-100 ppt) over India, the Indian Ocean, South
578 East Asia, the South China Sea and the Pacific Ocean, indicating transport by westerly winds.
579 The uniform increase in NO_X over India and China (Ind73 and Chin73) simulations show more
580 increase in ozone in the monsoon anticyclone in the case of Chinese emissions compared to
581 emissions from India. This is due to removal of NO_X by wet scavenging in the region near the

582 Himalayas. In the stratosphere, the impact of enhanced anthropogenic NO_X emissions is to
583 reduce ozone. ECHAM5-HAMMOZ simulations show a reduction in ozone in the stratosphere
584 (<70hPa). The highest ozone loss for the Ind38 simulation is ~0.5-2% in the stratosphere.
585
586

6. Conclusions

Analysis of PAN estimates from MIPAS satellite for the period 2002-2011 and ECHAM5-HAMMOZ global model simulations shows transport of boundary layer PAN into the monsoon anticyclone due to strong convection. The latitude-altitude, longitude-altitude cross-section maps reveals transport mainly occur from strong convections region of the South China Sea (~100-120E) and the southern flank of the Himalayas (~80-90E). These results are in agreement previous studies (Fu et al., 2006; Park et al., 2009; Fadnavis et al. ,2013; Chen et al., 2012) indicating significant vertical transport by deep convection and diabatic heating induced upwelling. Although the model simulations reproduce the main features, e.g. maximum in monsoon anticyclone and vertical transport into the UTLS, the MIPAS-E PAN is higher than model by ~30-60 ppt. The comparison of MIPAS-E PAN measurements with ACE-FTS indicates that MIPAS-E PAN is higher by ~70 ppt at the altitudes between 9.5–17.5 km (Tereszchuk et al., 2013).

The MIPAS-E PAN observations in the UTLS over India and China show annual trends in PAN varying between 0.4 ± 1.3 and 3.2 ± 0.49 ppt/year over India and 1 ± 0.25 and 3.4 ± 1.3 ppt/year over China. The seasonal trends are positive varying between 0.5± 0.8 and 2.7±0.47 ppt/year over India and 0.95 ± 1.2 and 2.9 ± 0.45 ppt/year over China. In general, the estimated trends are statistically significant at 2 sigma level except in the upper troposphere over India, where positive and negative trends are statistically insignificant. These statistically insignificant trends may be related to convective transport from the southern parts of the Himalaya and removal of NO_X by wet scavenging. Model simulations for enhanced NO_X emissions over India also show a non-linear increase in PAN in the upper troposphere. The estimated seasonal trends

610 are higher than annual trends at the altitude above 14 km over Indian, Chinese and ASM regions.
611 This may be due to transport by stronger deep convective activity during the monsoon season as
612 observed in radar, AVHRR, AIRS and MODIS (e.g Devasthale and Fueglistaler, 2010; Hassim
613 et al., 2014). The observed increasing frequency of over shooting convection over the tropical
614 land mass (Aumann and Ruzmaikin, 2013) indicate increasing trend in transport across the
615 tropical tropopause in agreement with our results. Quantification of changes in UTLS-PAN due
616 to overshooting convection is beyond the scope of this study. The trends estimated from
617 observations and model simulations are higher over China as compared to India, at the altitude
618 below 14 km and vice versa above 14 km. This may be related with the amount of pollution
619 outflow in the upper troposphere and lower stratosphere from India and China. The pollution
620 from China is released primarily below 14 km and Chinese emissions dominate over Indian
621 emissions. The pollution from India has substantial outflow above 14 km due to convective
622 lifting from southern slops of the Himalayas.

623

624 The trends estimated from sensitivity simulations for Ind38Chin73 are less than the
625 trends in MIPAS-E PAN as simulations does not account increase in VOCs. However it could
626 reproduce variations similar to MIPAS-E observations, higher trends values over the china
627 (compared to India) in the upper troposphere and vice versa in the lower stratosphere. The
628 sensitivity simulations for increase in NOx emissions over the Indian region lead to an increase
629 of PAN, HNO_3 and ozone over China and the western Pacific Ocean while increase in NO_X
630 emissions over China increases PAN over larger region covering India, South East Asia and
631 South China Sea, Indian Ocean and Pacific Ocean. Comparison of uniform increase in NO_X over

India and China (Ind73 and Chin73) shows that the effects on PAN, HNO_3 and O_3 mixing ratios in the anticyclone are more pronounced for Chinese emissions than for Indian emissions. Doubling (~1.9times) the NO_X emissions over India shows a non-linear increase in PAN, HNO_3 and O_3 over the ASM and the western pacific UTLS. The non linear response is related to transport pathways. Emissions over India are injected at the eastern end of monsoon anticyclone by the deep convection over the southern slopes of the Himalayas. Comparison of India and China simulations shows increase in NO_X over India result in less concentrations of PAN, HNO_3 over the Indian region especially near southern parts of the Himalaya, from where boundary layer Indian pollutants are transported into the monsoon anticyclone. The low concentration of PAN and HNO_3 over this region is due to removal of NO_X by wet scavenging. This may be due to higher efficiency of NOx conversion to HNO_3 over India compared to China. However, increase in NO_X emissions over China increases PAN and HNO_3 in the monsoon anticyclone. Part of these emissions is taken up by the westerly winds and is transported over the Pacific Ocean and as far as Atlantic. There is also westward transport by tropical easterlies which may explain part of the signal over the Atlantic Ocean in the tropics and the Southern Hemisphere. Cross-equatorial transport into the Southern Hemisphere over the south Indian Ocean occurs as well due to mixing by breaking Rossby waves around the equatorial tropopause and via the meridional overturning, or diabatic, circulation. This indicates that Chinese emissions have a greater impact on the concentrations of these species than Indian emissions.

Acknowledgements: The authors thank the High Power Computing Centre (HPC) in IITM, Pune, India, for providing computer resources. S. Fadnavis acknowledges with gratitude Prof. B. N. Goswami, Director of IITM, for his encouragement during the course of this study.

References

Alvarado, M. J., Logan, J. A., Mao, J., Apel, E., Riemer, D., Blake, D., Cohen, R. C., Min, K.-E., Perring, A. E., Browne, E. C., Wooldridge, P. J., Diskin, G. S., Sachse, G. W., Fuelberg, H., Sessions, W. R., Harrigan, D. L., Huey, G., Liao, J., Case-Hanks, A., Jimenez, J. L., Cubison, M. J., Vay, S. A., Weinheimer, A. J., Knapp, D. J., Montzka, D. D., Flocke, F. M., Pollack, I. B., Wennberg, P. O., Kurten, A., Crounse, J., J. Clair, M. St., Wisthaler, A., Mikoviny, T., Yantosca, R. M., Carouge, C. C., and Sager, P. Le: Nitrogen oxides and PAN in plumes from boreal fires during ARCTAS-B and their impact on ozone: an integrated analysis of aircraft and satellite observations, Atmos. Chem. Phys., 10, 9739–9760, doi:10.5194/acp-10-9739-2010, 2010.

Anderson, J.G., Wilmouth, D. M.,, Smith,J.B., and Sayres, D.S.: UV Dosage Levels in Summer: Increased Risk of Ozone Loss from Convectively Injected Water Vapor, Science,337, 835-839, 2012.

Aumann, H. H. and Ruzmaikin, A.: Frequency of deep convective clouds in the tropical zone from 10 years of AIRS data, Atmos. Chem. Phys., 13, 10795–10806, 2013.

Bhatt, B.C., Koh, T-Y, Yamamoto, M., and Nakamura, K.: The Diurnal Cycle of Convective Activity over South Asia as Diagnosed from METEOSAT-5 and TRMM Data, Terr. Atmos. Ocean. Sci., Vol. 21, No. 5, 841-854, doi: 10.3319/TAO.2010.02.04.01(A), 2010.

Chen, B., Xu, X. D., Yang, S., and Zhao, T. L.: Climatological perspectives of air transport from atmospheric boundary layer to tropopause layer over Asian monsoon regions during boreal summer inferred from Lagrangian approach, Atmos. Chem. Phys., 12, 5827–5839, 2012.

Choi Ki-Chul, Woo J-H , Kim H. K., Choi Jieun, Eum J-H and Baek B. H., Modeling of Emissions from Open Biomass Burning in Asia Using the BlueSky Framework, Asian Journal of Atmospheric Environment Vol. 7-1, pp.25-37, doi: http://dx.doi.org/10.5572/ajae.2013.7.1.025, 2013.

Cooper, O. R., Eckhardt, S., Crawford, J. H., Brown, C. C., Cohen, R. C., Bertram, T. H., Wooldridge, P., Perring, A., Brune, W.H., Ren, X., Brunner, D., and Baughcum, S. L.:

683 Summertime buildup and decay of lightning NOx and aged thunderstorm outflow above
684 North America, J. Geophys.Res., 114, D01101, doi:10.1029/2008JD010293, 2009.
685 Devasthale, A. and Fueglistaler, S.: A climatological perspective of deep convection penetrating
686 the TTL during the Indian summer monsoon from the AVHRR and MODIS instruments,
687 Atmos. Chem. Phys., 10, 4573–4582, doi:10.5194/acp-10-4573-2010, 2010.
688 Dodion, J., Fussen, D., Vanhellemont, F., Bingen, C., Mateshvili, N., Gilbert, K., Skelton, R.,
689 Turnball, D., McLeod, S. D., Boone, C. D., Walker, K. A., and Bernath P. F.: Aerosols
690 and clouds in the upper troposphere-lower stratosphere region detected by GOMOS and
691 ACE: Intercomparison and analysis of the years 2004 and 2005, Adv. Space Res., 42,
692 1730–1742, doi:10.1016/j.asr.2007.09.027, 2008.
693 Emmons, L. K., Hauglustaine, D. A., Muller, J.-F., Carroll, M. A., Brasseur, G. P., Brunner, D.,
694 Staehelin, J., Thouret, V. and Marenco A.: Data composites of tropospheric ozone and
695 its precursors from aircraft measurements, J. Geophys. Res., 105, 20,497 – 20,538, 2000.
696 Fadnavis, S., K. Semeniuk, L. Pozzoli, M. G. Schultz, S. D. Ghude, S. Das, and R. Kakatkar,
697 Transport of aerosols into the UTLS and their impact on the Asian monsoon region as
698 seen in a global model simulation, Atmos. Chem. Phys., 13, 8771–8786,
699 2013a,www.atmos-chem-phys.net/13/8771/2013/, doi:10.5194/acp-13-8771-2013.
700 Fadnavis, S., Semeniuk, K., Schultz, M. G., Mahajan, A.S., Luca Pozzoli, L., Sonbawane, S.,
701 Kiefer, M.: Transport Pathways of Peroxyacetyl Nitrate in the Upper Troposphere and
702 Lower Stratosphere from different monsoon systems during the Summer Monsoon
703 Season, Atmos. Chem. Phys. Discuss., 14, 20159-20195, doi:10.5194/acpd-14-20159-
704 2014, 2014.
705 Fiore, A. M., Horowitz, L. W., Purves, D. W., Levy II, H., Evans, M. J., Wang, Y., Li, Q., and
706 Yantosca, R. M.: Evaluating the contribution of changes in isoprene emissions to surface
707 ozone trends over the eastern United States, J. Geophys. Res., 110, D12303,
708 doi:10.1029/2004JD005485, 2005.

709 Fischer, E. V., Jacob, D. J., Yantosca, R. M., Sulprizio, M. P., Millet, D. B., Mao, J., Paulot, F.,
710 Singh, H. B., Roiger, A.-E., Ries, L., Talbot, R. W., Dzepina, K., and Pandey Deolal, S.:
711 Atmospheric peroxyacetyl nitrate (PAN): a global budget and source attribution, Atmos.
712 Chem. Phys. Discuss., 13, 26841–26891, 2013.

713 Fischer, H., Birk, M., Blom, C., Carli, B., Carlotti, M., von Clarmann, T., Delbouille, L., Dudhia,
714 A., Ehhalt, D., Endemann, M., Flaud, J. M., Gessner, R., Kleinert, A., Koopman, R.,
715 Langen, J., Lopez-Puertas, M., Mosner, P., Nett, H., Oelhaf, H., Perron, G., Remedios, J.,
716 Ridolfi, M., Stiller, G., and Zander, R.: MIPAS: an instrument for atmospheric and
717 climate research, Atmos. Chem. Phys., 8, 2151–2188, 2008, doi:10.5194/acp-8-2151-
718 2008.

719 Fischer, H. and Oelhaf, H.: Remote sensing of vertical profiles of atmospheric trace constituents
720 with MIPAS limb-emission spectrometers, Appl. Optics, 35, 2787–2796, 1996.

721 Fu, R., Hu, Y., Wright, J. S., Jiang, J. H., Dickinson, R. E., Chen, M., Filipiak, M., Read, W. G.,
722 Waters, J.W., and Wu, D. L.: Short circuit of water vapour and polluted air to the global
723 stratosphere by convective transport over the Tibetan Plateau, Proc Natl Acad Sci U S A.
724 Apr 11, 103(15), 5664-9, Epub Apr 3, 2006.

725 Ganzeveld, L., and Lelieveld, J.: Dry deposition parameterization in a chemistry general
726 circulation model and its influence on the distribution of reactive trace gases, J. Geophys.
727 Res.,100(D10), 20999–21012, doi:10.1029/95JD02266, 1995.

728 Gettelman, A., Kinnison, D. E., Dunkerton, T. J., and Brasseur, G. P.: The impact of monsoon
729 circulations on the upper troposphere and lower stratosphere, J. Geophys. Res., 109,
730 D22101, doi:10.1029/2004JD004878, 2004.

731 Ghude, S. D, Kulkarni, S. H., Jena, C., Pfister, G. G., Beig, G., Fadnavis, S., and van der A R. J.,
732 Application of satellite observations for identifying regions of dominant sources of
733 nitrogen oxides over the Indian Subcontinent, J. Geophys. Res., 118, 1–15,
734 doi:10.1029/2012JD017811, 2013.

Glatthor, N., Von Clarmann T., Fischer, H., Funke, B., Grabowski, U., Höpfner, M., Kellmann, S., Kiefer, M., Linden, A., Milz, M., Steck, T., and Stiller, G.P.: Global peroxyacetyl nitrate (PAN) retrieval in the upper troposphere from limb emission spectra of the Michelson Interferometer for Passive Atmospheric Sounding (MIPAS), Atmos. Chem. Phys., 7, 2775-2787, www.atmos-chem-phys.net/7/2775/2007/ doi:10.5194/acp-7-2775-2007, 2007.

Hassim, M. E. E., Lane, T. P., and May, P. T.: Ground-based observations of overshooting convection during the Tropical Warm Pool-International Cloud Experiment, J. Geophys. Res. Atmos.,119, 880–905, doi:10.1002/2013JD020673, 2014.

Hilboll, A., Richter, A. and Burrows, J. P.: Long-term changes of tropospheric NO_2 over megacities derived from multiple satellite instruments, Atmos. Chem. Phys., 13, 4145-4169, 2013, www.atmos-chem-phys.net/13/4145/2013/, doi:10.5194/acp-13-4145-2013.

Holland, E. A., and Lamarque J. F.: Modeling bio-atmospheric coupling of the nitrogen cycle through NOx emissions and NOy deposition, Nutr. Cycl. Agroecosyst., 48, 7 – 24, 1997.

Horowitz, L. W., Walters, S., Mauzerall, D. L., Emmons, L. K., Rasch, P. J., Granier, C., Tie, X., Lamarque, J., Schultz, M. G.,Tyndall, G. S., Orlando, J. J., and Brasseur, G. P.: A global simulation of tropospheric ozone and related tracers, Description and evaluation of MOZART, version 2, J. Geophys. Res., 108, 4784, doi:10.1029/2002JD002853, 2003.

Jiang, J. H., Livesey, N. J., Su, H., Neary, L., McConnell, J. C., and Richards, N. A. D.: Connect, ing surface emissions, convective uplifting, and long-range transport of carbon monoxide in 20 the upper troposphere: New observations from the Aura Microwave Limb Sounder, Geophys. Res. Lett., 34, L18812, doi:10.1029/2007GL030638, 2007.

Keim, C., Liu, G. Y., Blom, C. E., Fischer, H., Gulde, T., Höpfner, M., Piesch, C., Ravegnani, F., Roiger, A., Schlager, H., and Sitnikov, N.: Vertical profile of peroxyacetyl nitrate (PAN) from MIPAS-STR measurements over Brazil in February 2005 and its contribution to tropical UT NO_y partitioning, Atmos. Chem. Phys., 8, 4891-4902, www.atmos-chem-phys.net/8/4891/2008/ doi:10.5194/acp-8-4891-2008, 2008.

762 Labrador, L. J., von Kuhlmann, R., and Lawrence, M. G:: The effects of lightning-produced
763 NOx and its vertical distribution on atmospheric chemistry: sensitivity simulations with
764 MATCH-MPIC, Atmos. Chem. Phys., 5, 1815–1834, 2005.
765 Li, Q., Jiang, J. H., Wu, D. L., Read, W. G., Livesey, N. J.,. Waters, J. W:, Zhang, Y., Wang, B.,
766 Filipiak, M. J., Davis, C. P., Turquety, S., Wu, S., Park R. J., Yantosca R. M., and Jacob
767 D. J.: Convective outflow of South Asian pollution: A global CTM simulation compared
768 with EOS MLS observations, Geophys. Res. Lett., 32, L14826,
769 doi:10.1029/2005GL022762, 2005.
770 Nesbitt, S.W., Zhang, R., and Orville, R. E.: Seasonal and global NO*x* production by lightning
771 estimated from the optical transient detector (OTD), Tellus B **52**, 1206–1215, 2000.
772 Nowak, J., Parris, D. D., Neuman, J. A., Holloway, J. S., Cooper. O. R., Ryerson, T. B., Nicks,
773 D. K., Flocke, F., Roberts, J. M., Atlas, E., de Gouw, J. A., Donnelly, S., Dunlea, E.,
774 Hubler, G., Huey, L. G., Schauffler, S., Tanner, D. J., Warneke, C., and Fehsenfeld, F. C.
775 S.: Gas-phase chemical characteristics of Asian emission plumes observed during ITCT
776 2K2 over the eastern North Pacific Ocean, J. Geophys. Res., 109, D23S19,
777 doi:10.1029/2003JD004488, 2004.
778 Ohara, T., Akimoto, H.,. Kurokawa J, Horii N., Yamaji K., Yan X., and Hayasaka T.: An Asian
779 emission inventory of anthropogenic emission sources for the period 1980–2020, Atmos.
780 Chem. Phys., 7, 4419–4444, www.atmos-chem-phys.net/7/4419/2007, 2007.
781 Park, M., Randel, W. J., Emmons, L. K., and Livesey, N. J.: Transport pathways of carbon
782 monoxide in the Asian summer monsoon diagnosed from Model of Ozone and Related
783 Tracers (MOZART), J. Geophys. Res., 114, D08303, doi:10.1029/2008JD010621, 2009.
784 Park M., Randel, W. J., Emmons, L. K., Bernath, P. F., Walker, K. A. and Boone, C. D.:
785 Chemical isolation in the Asian monsoon anticyclone observed in Atmospheric
786 Chemistry Experiment (ACE-FTS) data, Atmos. Chem. Phys., 8, 757–764, 2008.

787 Park, M., Randel, W. J., Getteleman, A., Massie, S. T., and Jiang, J. H.: Transport above the
788 Asian summer monsoon anticyclone inferred from Aura Microwave Limb Sounder
789 tracers, J. Geophys. Res., 112, D16309, doi:10.1029/2006JD008294, 2007.
790 Park, M., Randel, W. J., Kinnison, D. E., Garcia, R. R., and Choi, W.: Seasonal variation of
791 methane, water vapour, and nitrogen oxides near the tropopause: Satellite observations
792 and model simulations, J. Geophys. Res., doi:10.1029/2003JD003706, 109, D03302,
793 2004.
794 Penki, R.K. and Kamra A. K., Lightning distribution with respect to the monsoon trough position
795 during the Indian summer monsoon season, J. Geophy. Res., 118, 4780–4787,
796 doi:10.1002/jgrd.50382, 2013.
797 Pozzoli, L., Bey, I., Rast, J. S., Schultz, M. G., Stier, P., and Feichter, J.: Trace gas and aerosol
798 interactions in the fully coupled model of aerosol-chemistry-climate ECHAM5-
799 HAMMOZ: 1. Model description and insights from the spring 2001 TRACE-P
800 experiment, J. Geophys. Res., 113, D07308, doi:10.1029/2007JD009007, 2008a.
801 Pozzoli, L., Bey, I., Rast, J. S., Schultz, M. G., Stier, P., and Feichter, J.: Trace gas and aerosol
802 interactions in the fully coupled model of aerosol-chemistry-climate ECHAM5-
803 HAMMOZ: 2. Impact of heterogeneous chemistry on the global aerosol distributions, J.
804 Geophys. Res., 113, D07309, doi:10.1029/2007JD009008, 2008b.
805 Pozzoli, L., Janssens-Maenhout, G., Diehl, T., Bey, I., Schultz, M. G., Feichter, J., Vignati, E.,
806 and Dentener, F.: Re-analysis of tropospheric sulfate aerosol and ozone for the period
807 1980–2005 using the aerosol-chemistry-climate model ECHAM5-HAMMOZ, Atmos.
808 Chem. Phys., 11, 9563-9594, doi:10.5194/acp-11-9563-2011, 2011.
809 Ranalkar M. R and Chaudhari, H. S.: Seasonal variation of lightning activity over the Indian
810 subcontinent. Meteorology and Atmospheric Physics, 104,125–134, 2009.
811 Randel W. J. and Jensen E. J.: Physical processes in the tropical tropopause layer and their roles
812 in a changing climate, Nature Geoscience, 6,169–176, doi:10.1038/ngeo1733, 2013.
813 Randel, W. J., and Park, M.: Deep convective influence on the Asian summer monsoon
814 anticyclone and associated tracer variability observed with Atmospheric Infrared Sounder
815 (AIRS), J. Geophys. Res., 111, D12314, doi:10.1029/2005JD006490, 2006.

816 Randel, W. J., Park, M., Emmons, L., Kinnison, D., Bernath, P., Walker, K. A., Boone, C., and
817 Pumphrey H.: Asian monsoon transport of pollution to the stratosphere, Science. Apr
818 30,328(5978),611-3. Epub Mar 25, 2010.
819 Ravishankara A. R., Water Vapor in the Lower Stratosphere, Science Vol. 337, no. 6096, pp.
820 809-810 DOI: 10.1126/science.1227004, 2012.
821 Ridley, B. A., Madronich, S., Chatfield, R. B., Walega, J. G., Shetter, R. E., Carroll, M. A., and
822 Montzka, D. D: Measurements and model simulations of the photostationary state during
823 the Mauna Loa Observatory Photochemistry Experiment: Implications for radical
824 concentrations and ozone production and loss rates, J. Geophys. Res., 97(D10), 10375–
825 10388, doi:10.1029/91JD02287, 1992.
826 Roeckner, E., Bauml, G., Bonaventura, L., Brokopf, R., Esch, M., Giorgetta, M., Hagemann, S.,
827 Kirchner, I., Kornblueh, L., Manzini, E., Rhodin, A., Schlese, U., Schulzweida, U., and
828 Tompkins, A.: The atmospehric general circulation model ECHAM5: Part 1, Tech. Rep.
829 349, Max Planck Institute for Meteorology, Hamburg, 2003.
830 Sander, S. P., Fried, R. R., Barker, J. R., Golden, D. M., Kurylo, M. J.,Wine, P. H., J. Abbatt, P.
831 D., 25 Burkholder, J. B., Kolb, C. E., Moortgat, G. K., Huie, R. E., and Orkin, V. L.:
832 Chemical kinetics and photochemical data for use in atmospheric studies, evaluation
833 number 14, JPL Publ. 02-25, Jet Propul. Lab., Calif. Inst. of Technol., Pasadena,
834 available at: http://jpldataeval.jpl. nasa.gov/pdf/JPL_02-25_rev02.pdf, 2003.
835 Sander, S. P., Finlayson-Pitts, B. J., Friedl, R. R., Golden, D. M., Huie, R. E., Keller-Rudek, H.,
836 30 Kolb, C. E., Kurylo, M. J., Molina, M. J., Moortgat, G. K., Orkin, V. L.,
837 Ravishankara, A. R., and Wine, P. H.: Chemical Kinetics and Photochemical Data for
838 Use in Atmospheric Studies, Evaluation Number 15, JPL Publication 06-2, Jet Propulsion
839 Laboratory, Pasadena, available at: http://jpldataeval.jpl.nasa.gov (last access: July 2006),
840 2006.

841 Schneider, P. and van der A. R. J.:, A global single-sensor analysis of 2002–2011 tropospheric
842 nitrogen dioxide trends observed from space, J, Geophy. Res., 117, D16309,
843 doi:10.1029/2012JD017571, 2012.

844 Shepon, A., Gildor, H., Labrador, L. J., Butler, T., Ganzeveld, L. N., and Lawrence, M. G.:
845 Global reactive nitrogen deposition from lightning NOx, J. Geophys. Res., 112, D06304,
846 doi:10.1029/2006JD007458, 2007.

847 Singh, H. B., Viezee, W., Chen, Y., Thakur, A. N., Kondo, Y. and Talbot, R. W.,Gregory, G. L.,
848 Sachse, G. W., Blake, D. R., Bradshaw, J. D., Wang, Y., and Jacob D. J.: Latitudinal
849 distribution of reactive nitrogen in the free troposphere over the Pacific Ocean in late
850 winter/early spring, J. Geophys. Res., 103(D21), 28237–28246, doi:10.1029/98JD01891,
851 1998.

852 Sinha V., Kumar V., and Sarkar C.:Chemical composition of pre-monsoon air in the Indo–
853 Gangetic Plain measured using a new PTR-MS and air quality facility: high surface
854 ozone and strong influence of biomass burning, Atmos. Chem. Phys. Discuss., 13, 31761-
855 31813, www.atmos-chem-phys-discuss.net/13/31761/2013/, doi:10.5194/acpd-13-31761-
856 2013, 2013.

857 Stier, P., Feichter, J., Kinne, S., Kloster, S., Vignati, E., Wilson, J., Ganzeveld, L., Tegen, I.,
858 Werner, M., Balkanski, Y., Schulz, M., Boucher, O., Minikin, A., and Petzold, A.: The
859 aerosol-climate model ECHAM5-HAM, Atmos. Chem. Phys., 5, 1125–1156,
860 doi:10.5194/acp-5-1125-2005, 2005.

861 Tereszchuk, K. A., Moore, D. P., Harrison, J. J., Boone, C. D., Park, M., Remedios, J. J., Randel,
862 W. J., and Bernath, P. F.: Observations of peroxyacetyl nitrate (PAN) in the upper
863 troposphere by the Atmospheric Chemistry Experiment Fourier Transform Spectrometer
864 (ACE-FTS), Atmos. Chem. Phys., 13, 5601–5613, www.atmos-chem-
865 phys.net/13/5601/2013/, doi:10.5194/acp-13-5601-2013, 2013.

Tie X., Zhang, R., Brasseur, G., and Lei, W.: Global NO*x* Production by Lightning, Journal of Atmospheric Chemistry 43: 61–74, 2002.

Tie, X.X., Zhang, R., Brasseur, G., Emmons, L. and Lei, W.: Effects of lightning on reactive nitrogen and nitrogen reservoir species in the troposphere. *Journal of Geophysical Research-Atmospheres*, **106**, 3167-3178, DOI: 10.1029/2000JD900565, 2001.

Vernier, J. P., Thomason, L. W., and Kar, J.: CALIPSO detection of an Asian tropopause aerosol layer, Geophys. Res. Lett., 38, L07804, doi:10.1029/2010GL046614, 2011.

Von Clarmann, T., Höpfner, M., Kellmann, S., Linden, A., Chauhan, S., Funke, B., Grabowski, U.,Glatthor, N., Kiefer, M., Schieferdecker, T., Stiller, G. P., and Versick, S.: Retrieval of temperature, H2O, O3, HNO_3, CH_4, N_2O, $ClONO_2$ and ClO from MIPAS reduced resolution nominal mode limb emission measurements, Atmos. Meas. Tech., 2, 159–175, doi:10.5194/amt-2- 2159-2009, 2009.

Wiegele, A., Glatthor, N., Hopfner, M., Grabowski ,U., Kellmann, S., Linden, A., Stiller, G., and von Clarmann, T.: Global distributions of C_2H_6, C_2H_2, HCN, and PAN retrieved from MIPAS reduced spectral resolution measurements, Atmos. Meas. Tech., 5, 723–734, doi:10.5194/amt-5-723-2012, 2012.

Walker, T. W., Martin, R. V., Donkelaar, A. van, Leaitch, W. R., MacDonald, A. M., Anlauf, K. G., Cohen, R. C., Bertram, T. H., Huey, L. G., Avery, M. A., Weinheimer, A. J., Flocke, F. M., Tarasick, D. W., Thompson, A. M., Streets, D. G., and Liu, X.: Trans-Pacific transport of reactive nitrogen and ozone to Canada during spring, Atmos. Chem. Phys., 10, 8353–8372, www.atmos-chem-phys.net/10/8353/2010/, 2010.

Wu, Z., Wang, X., Turnipseed, A. A., Chen, F, Zhang, L., Guenther, A. B., Karl, T., Huey, L. G., 25 Niyogi, D., Xia, B., and Alapaty, K.: Evaluation and improvements of two community models in simulating dry deposition velocities for peroxyacetyl nitrate (PAN) over a coniferous forest, J. Geophys. Res., 117, D04310, doi:10.1029/2011JD016751, 2012..

Xiong, X., Houweling, S., Wei, J., Maddy, E., Sun, F., and Barnet, C.: Methane plume over South Asia during the monsoon season: Satellite observation and model simulation, Atmos. Chem. Phys., 9, 783– 794, 2009.

894 Yang, X. and Z. Li, Z.: Increases in thunderstorm activity and relationships with air pollution in
895 southeast China, J. Geophys. Res. Atmos., 119, 1835–1844, doi:10.1002/2013JD021224,
896 2014.

897 Yamaji, K., Ohara, T., Uno, I., Tanimoto, H., Kurokawa, J., Akimoto, H.:. Analysis of the
898 seasonal variation of ozone in the boundary layer in East Asia using the Community
899 Multi-scale Air Quality model: what controls surface ozone levels over Japan?
900 Atmospheric Environment 40, 1856e1868, 2006.

901 Zhao, C., Wang, Y., Choi, Y., and Zeng, T.: Summertime impact of convective transport and
902 lightning NOx production over North America: modeling dependence on meteorological
903 simulations, Atmos. Chem. Phys., 9, 4315–4327, www.atmos-chem-
904 phys.net/9/4315/2009/, 2009.

905

906 Table 1: Global aircraft measurements used for model evaluation.

Experiment	Date Frame	Species	Location
POLINAT-2 (Falcon)	Sep 19-Oct 25, 1997	O3, NOX	Canary-Islands:LAT= 25., 35. LON=340., 350. E-Atlantic:LAT= 35., 45.LON=330.,340. Europe: LAT= 45.,55. LON=5.,15. Ireland: LAT=50., 60. LON= 345.,355.
PEM-Tropics-A (DC8)	Aug 24-Oct 15, 1996	O3, NOX, HNO3, PAN	Christmas-Island: LAT= 0., 10. LON=200., 220. Easter-Island: LAT=-40.,-20.LON=240., 260. Fiji: LAT= -30.,-10. LON= 170., 190. Hawaii: LAT= 10., 30. LON= 190., 210. Tahiti: LAT= -20., 0. LON= 200., 230.
PEM-Tropics-A (P3)	Aug 15-Sep 26, 1996	O3, HNO3	Christmas-Island: LAT= 0., 10. LON= 200., 220. Easter-Island: LAT= -40.,-20. LON= 240., 260. Hawaii: LAT= 10., 30. LON= 190., 210. Tahiti: LAT= -20., 0. LON= 200., 230.
ABLE-3B (Electra)	Jul 6-Aug 15, 1990	O3, NOX, HNO3, PAN	Labrador: LAT= 50., 55. LON= 300., 315. Ontario: LAT= 45., 60. LON= 270., 280. US-E-Coast: LAT= 35., 45. LON= 280., 290.
CITE-3 (Electra)	Aug 22-Sep 29, 1989	O3, NOX	Natal: LAT= -15.,5. LON= 325., 335. Wallops: LAT= 30., 40. LON= 280., 290.
ELCHEM (Sabreliner)	Jul 27-Aug 22, 1989	O3, NOX	New-Mexico: LAT=30., 35. LON= 250., 255.
ABLE-3A (Electra)	Jul 7-Aug 17, 1988	O3, NOX ,PAN	Alaska: LAT= 55., 75. LON= 190., 205.
ABLE-2A (Electra)	Jul 12-Aug 13, 1985	O3	E-Brazil: LAT= -10., 0. LON= 300., 315. W-Brazil: LAT= -5., 0. LON= 290., 300.
STRATOZ-3 (Caravelle 116)	Jun 4-26, 1984	O3	Brazil: LAT= -20.,0. LON= 315., 335. Canary-Islands: LAT= 20.,35. LON= 340., 355. E-Tropical-N-Atlantic: LAT= 0.,20.LON=330.,345. England: LAT= 45., 60. LON= -10., 5. Goose-Bay: LAT= 45., 60. LON= 290., 305. Greenland: LAT= 60., 70. LON= 290., 330. Iceland: LAT= 60., 70. LON= 330., 355. NW-South-America: LAT=-5., 10. LON= 275.,295. Puerto-Rico: LAT= 10., 25. LON= 290., 300. S-South-America: LAT= -65.,-45. LON= 275., 300. SE-South-America: LAT= -45.,-20. LON= 295.,320. SW-South-America: LAT=-45.,-25. LON= 285.,292. Spain: LAT= 35., 45. LON= -15., 0. W-Africa: LAT= 0., 15. LON= -15., 0. W-South-America: LAT= -25., -5. LON= 275.,290. Western-N-Atlantic: LAT= 25., 45.LON= 290.,300.
CITE-2 (Electra)	Aug 11-Sep 5, 1986	O3, NOX, HNO3, PAN	Calif: LAT= 35., 45. LON= 235., 250. Pacific: LAT= 30., 45. LON= 225., 235.
CAIPEEX	Sep 2009 and oct 2010	O3, NOX	Lat=17^0N, Lon=78^0E

907

908

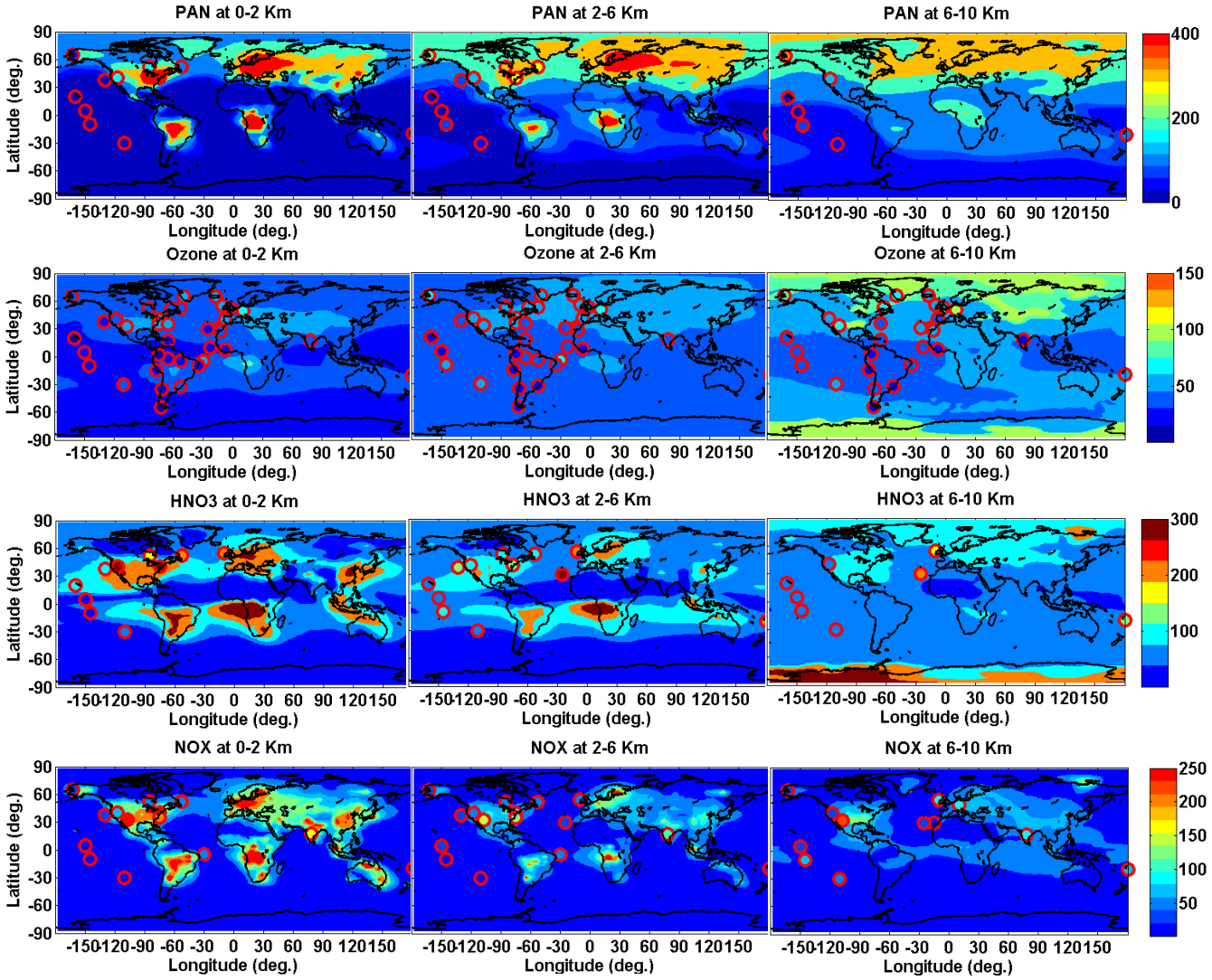

Figure 1 Global mean distribution of PAN (ppt), ozone (ppb), HNO_3 (ppt), NO_X (ppt) averaged for the monsoon season and altitude ranges. Model results from reference simulation (background solid contours) are compared with aircraft observations from Table 1 for all the years (filled circles). Aircraft observations are averaged vertically and horizontally over the coherent regions.

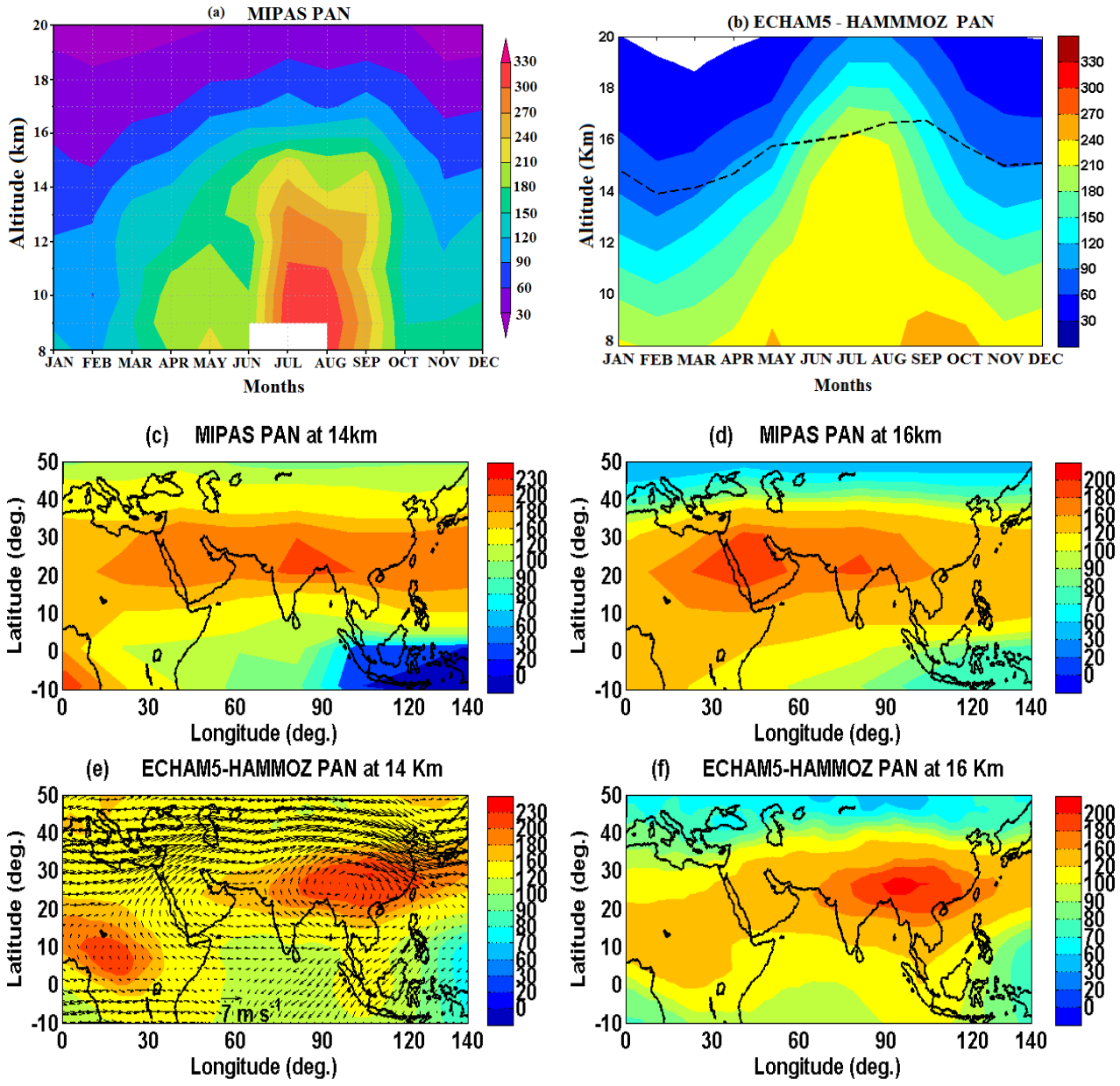

Figure 2. The monthly distribution of PAN (ppt) averaged over anticyclone region (60-120^{O}E, 10-40^{O}N) (a) as observed by MIPAS and for the period 2002-2011 (b) ECHAM5-HAMMOZ reference simulation. Distribution of seasonal mean PAN concentration (ppt) as observed by MIPAS (climatology for the period 2002-2011) at (c) 14 km (d) 16 km and ECHAM5-HAMMOZ reference simulation at (e)14 km (f) 16 km. ECHAM5-HAMMOZ simulation is smoothed with averaging kernel of MIPAS.

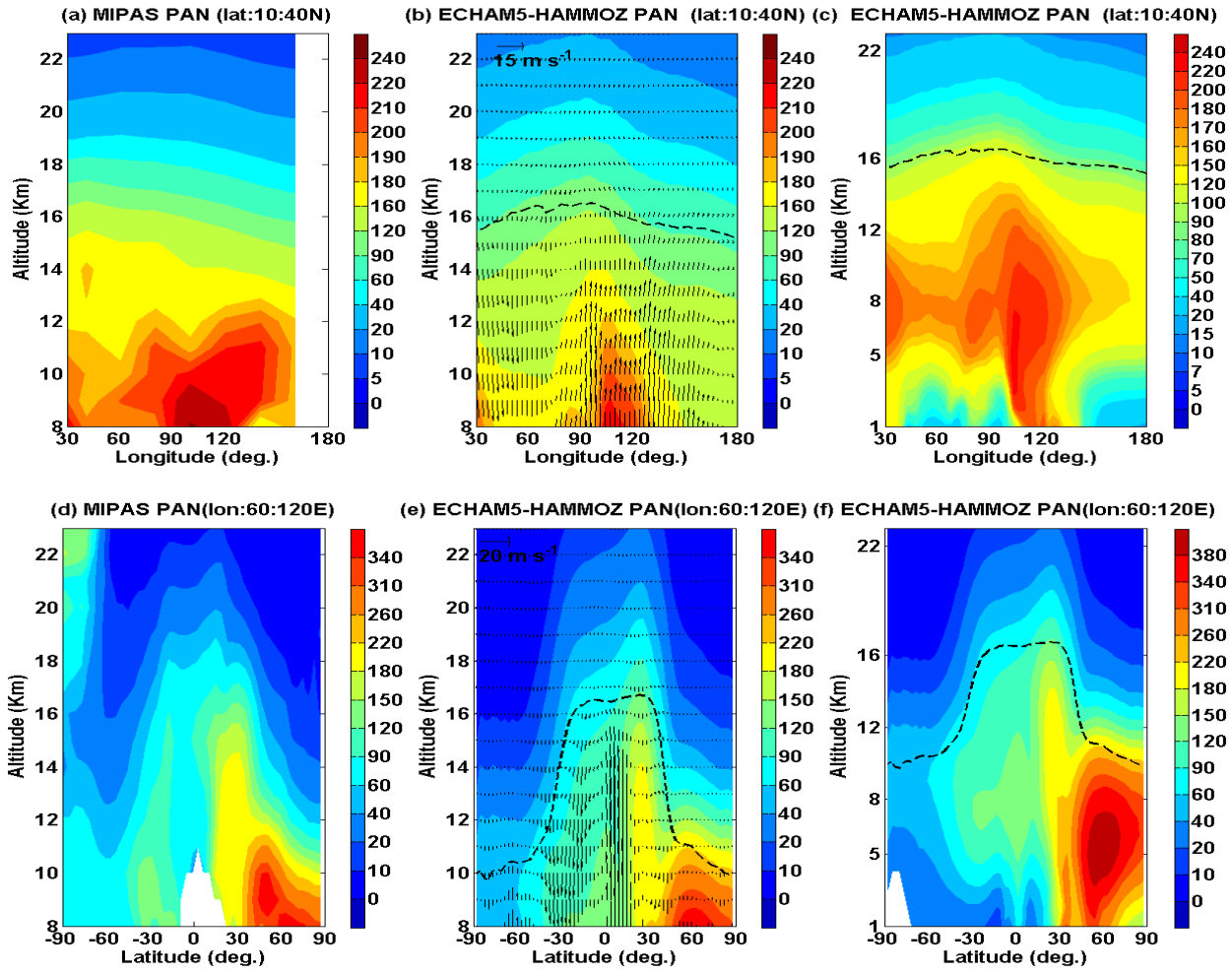

Figure 3: Longitude-altitude cross section of PAN (ppt) averaged for the monsoon season and 10-40^{O}N (a) MIPAS (climatology for the period 2002-2011) (b) ECHAM5-HAMMOZ reference simulation between 8-23km. The black arrows indicate wind vectors. The vertical velocity field has been scaled by 300. (c) same as figure (b) but from the surface. Latitude- altitude cross section of PAN (ppt) averaged for the monsoon season and 60-120^{O}E (d) MIPAS climatology (e) ECHAM5-HAMMOZ reference simulation between8-23km, (f) same as figure (e) but from the surface. ECHAM5-HAMMOZ simulation is smoothed with averaging kernel of MIPAS.

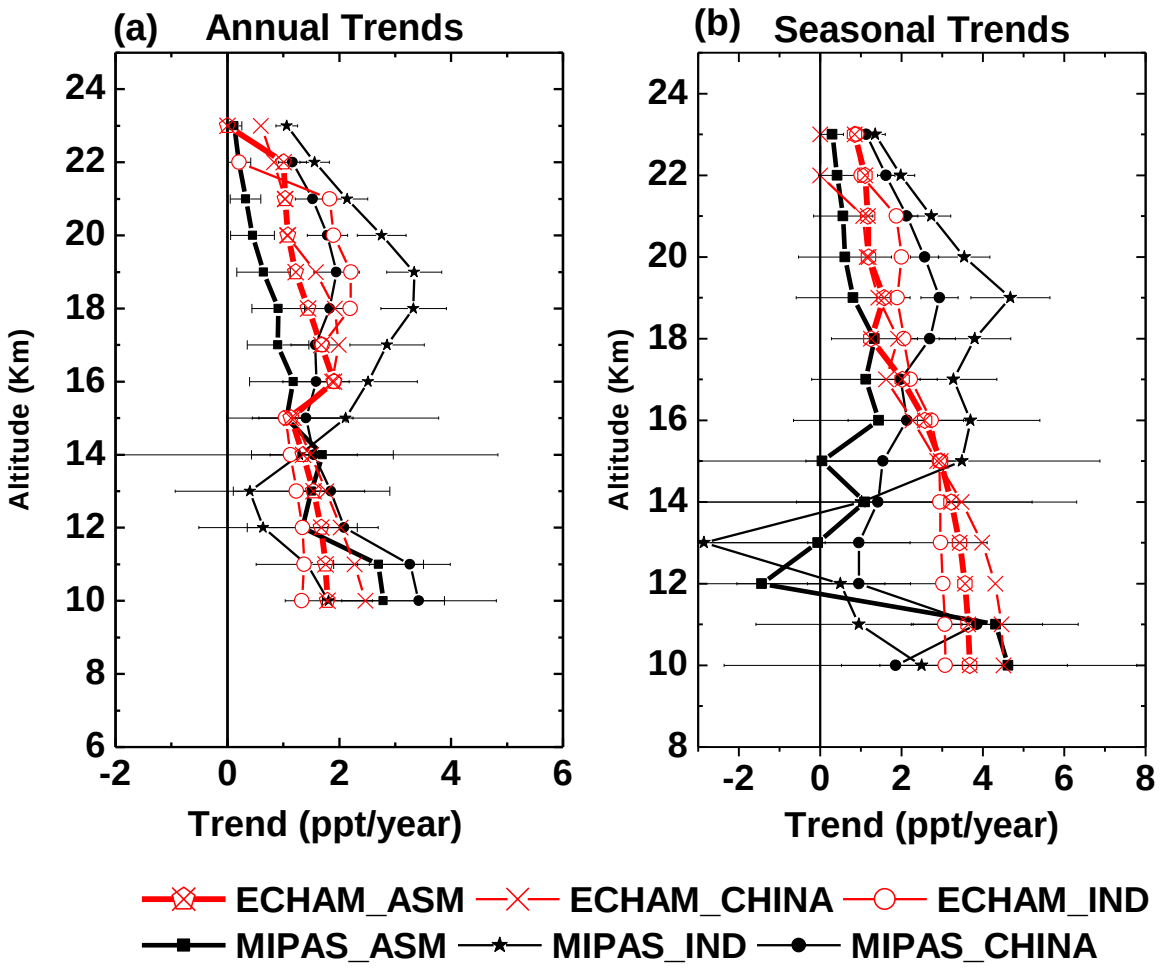

Figure 4: Vertical variation of trends obtained from monthly mean MIPAS-E PAN concentrations averaged for the period 2002-2011 and Ind38Chin73 simulations over the Asian summer monsoon region, China and India (a) annual trends (b) seasonal (June-September) trends.

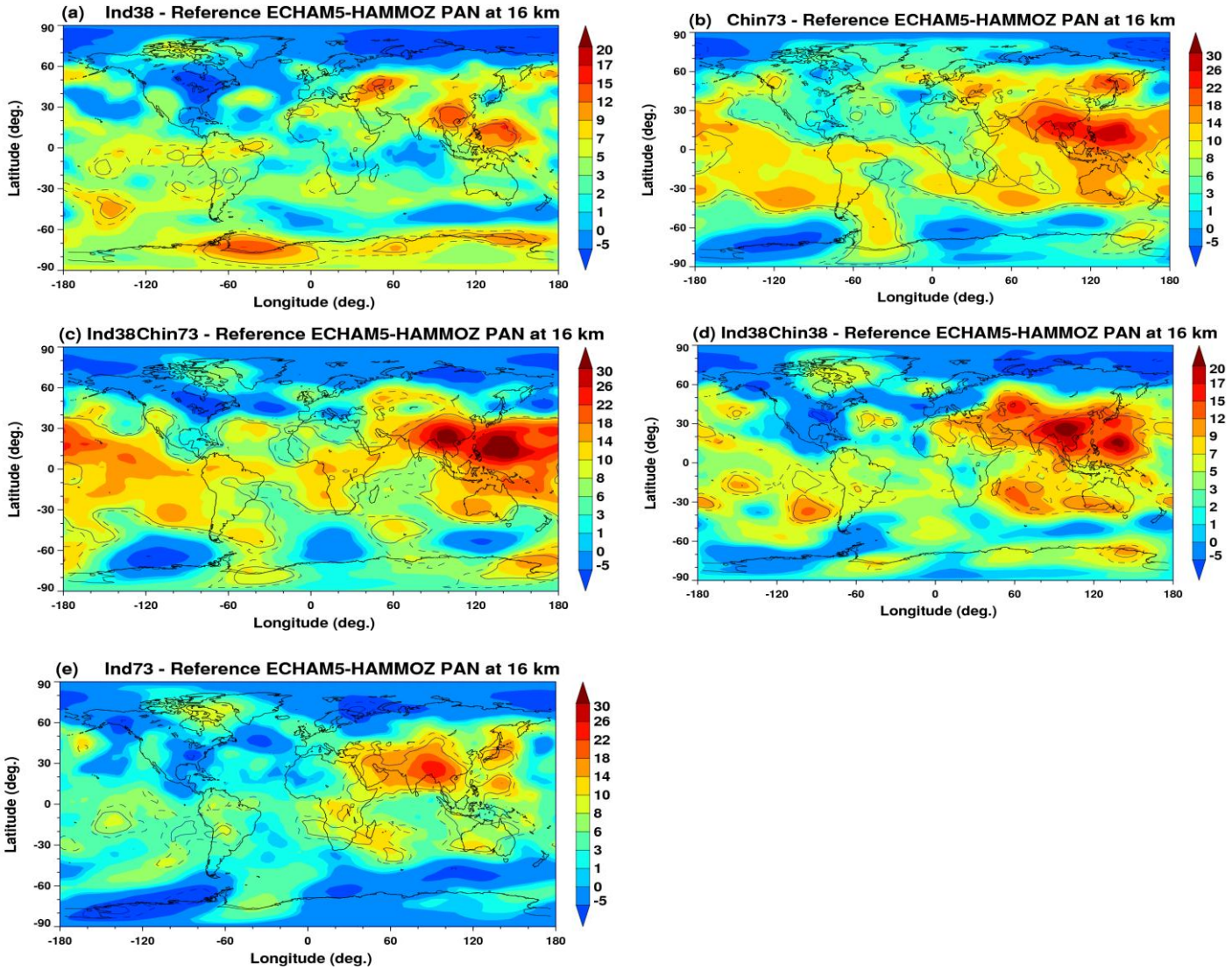

Figure 5 Percentage change in ECHAM5-HAMMOZ PAN at 16km , as obtained from (a) Ind38 (b) Chin73 (c) Ind38Chin73 (d) Ind38Chin38 and (e) Ind73 simulations. Solid black line indicates the 95% Student's t test confidence interval while dashed line indicates 90% confidence interval.

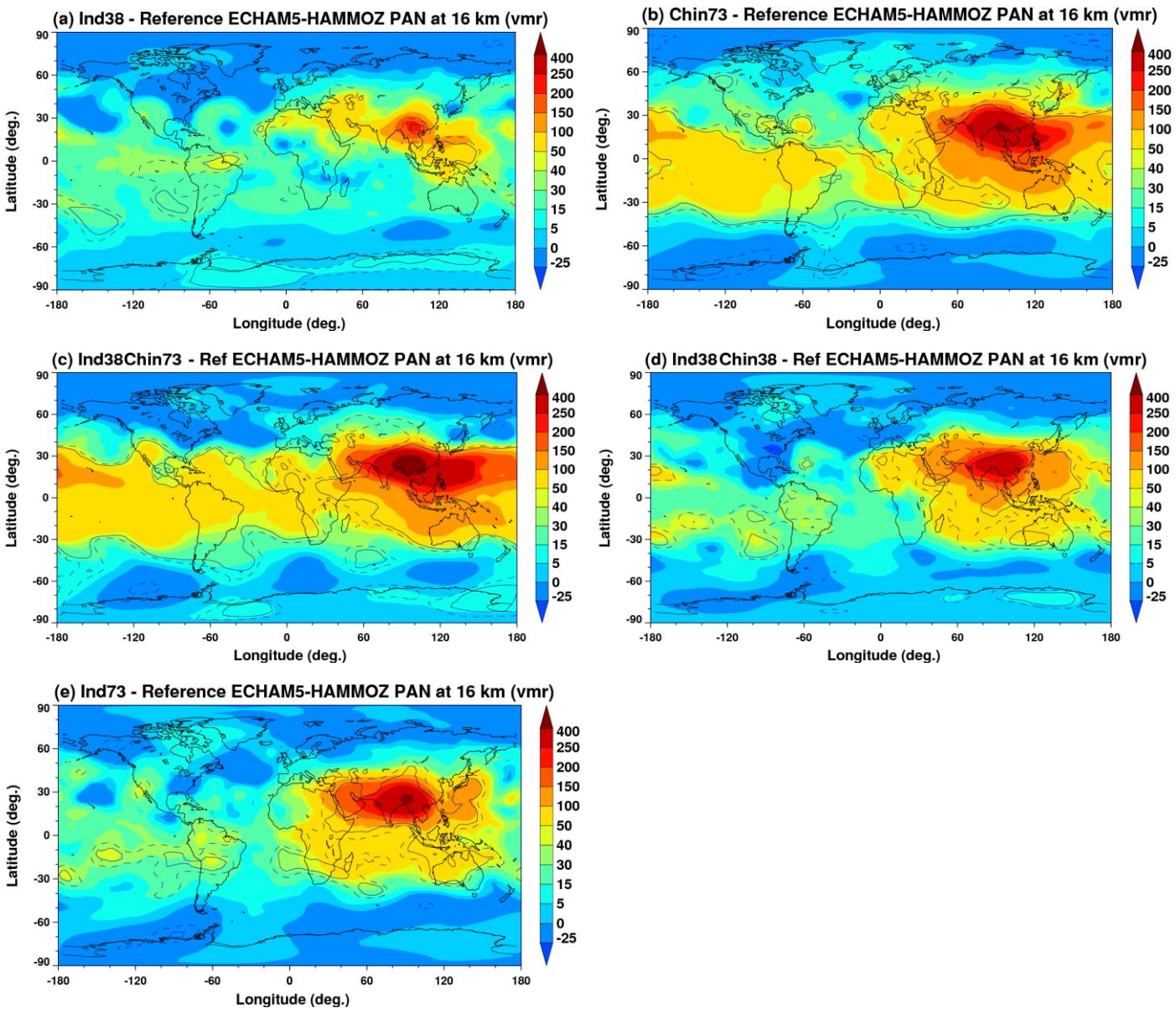

Figure 6 Change in ECHAM5-HAMMOZ PAN at 16km in ppt, as obtained from (a) Ind38 (b) Chin73 (c) Ind38Chin73 (d) Ind38Chin38 and (e) Ind73 simulations. Solid black line indicates the 95% Student's t test confidence interval while dashed line indicates 90% confidence interval.

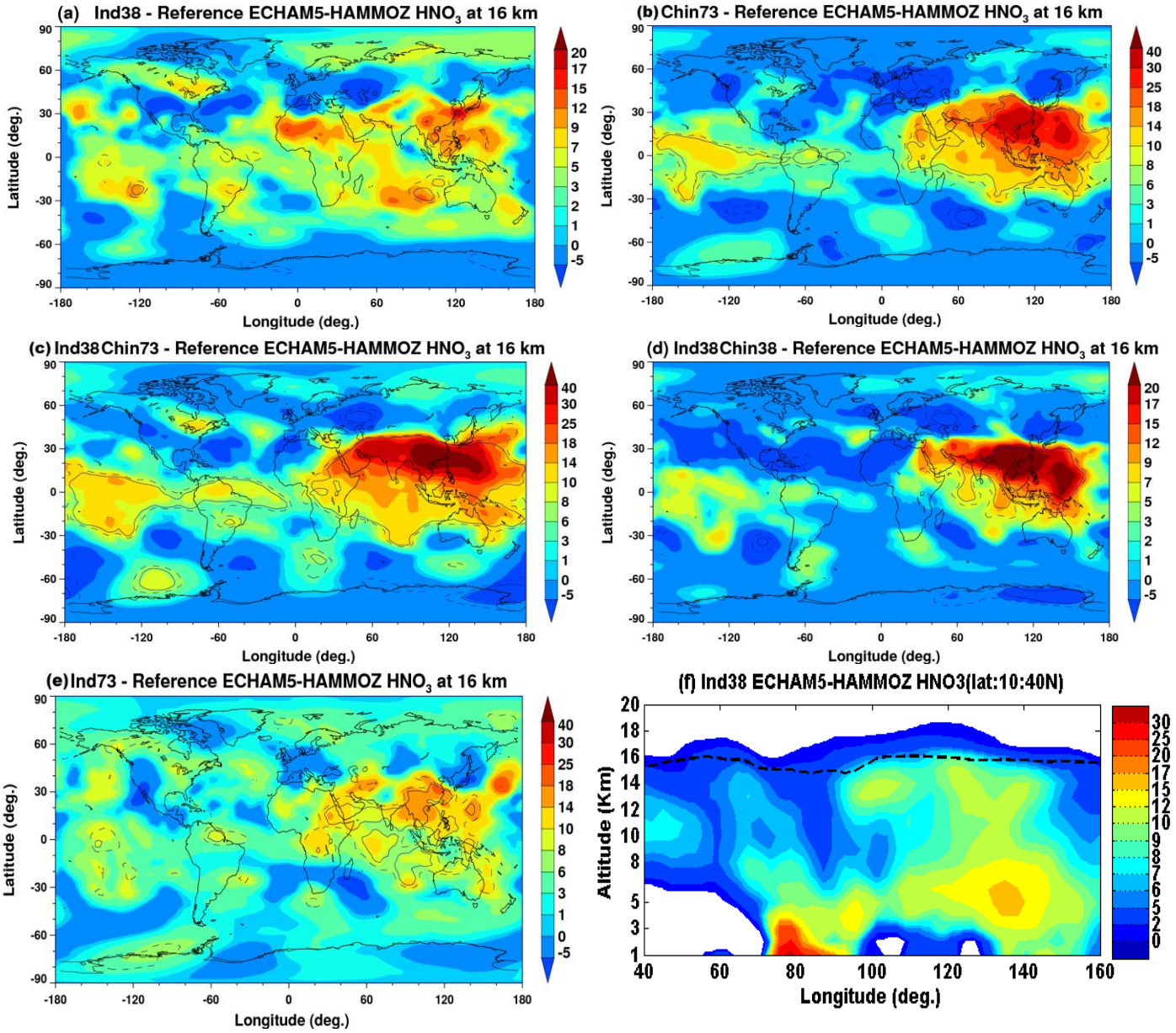

Figure 7 Percentage change in ECHAM5-HAMMOZ HNO_3 at 16km, as obtained from (a) Ind38 (b) Chin73 (c) Ind38Chin73 (d) Ind38Chin38 and (e) Ind73 simulations. Solid black line indicates the 95% Student's t test confidence interval while dashed line indicates 90% confidence interval (f) Longitude-altitude cross section (averaged over 0-40N) of percentage change in HNO_3 for Ind38 simulation.

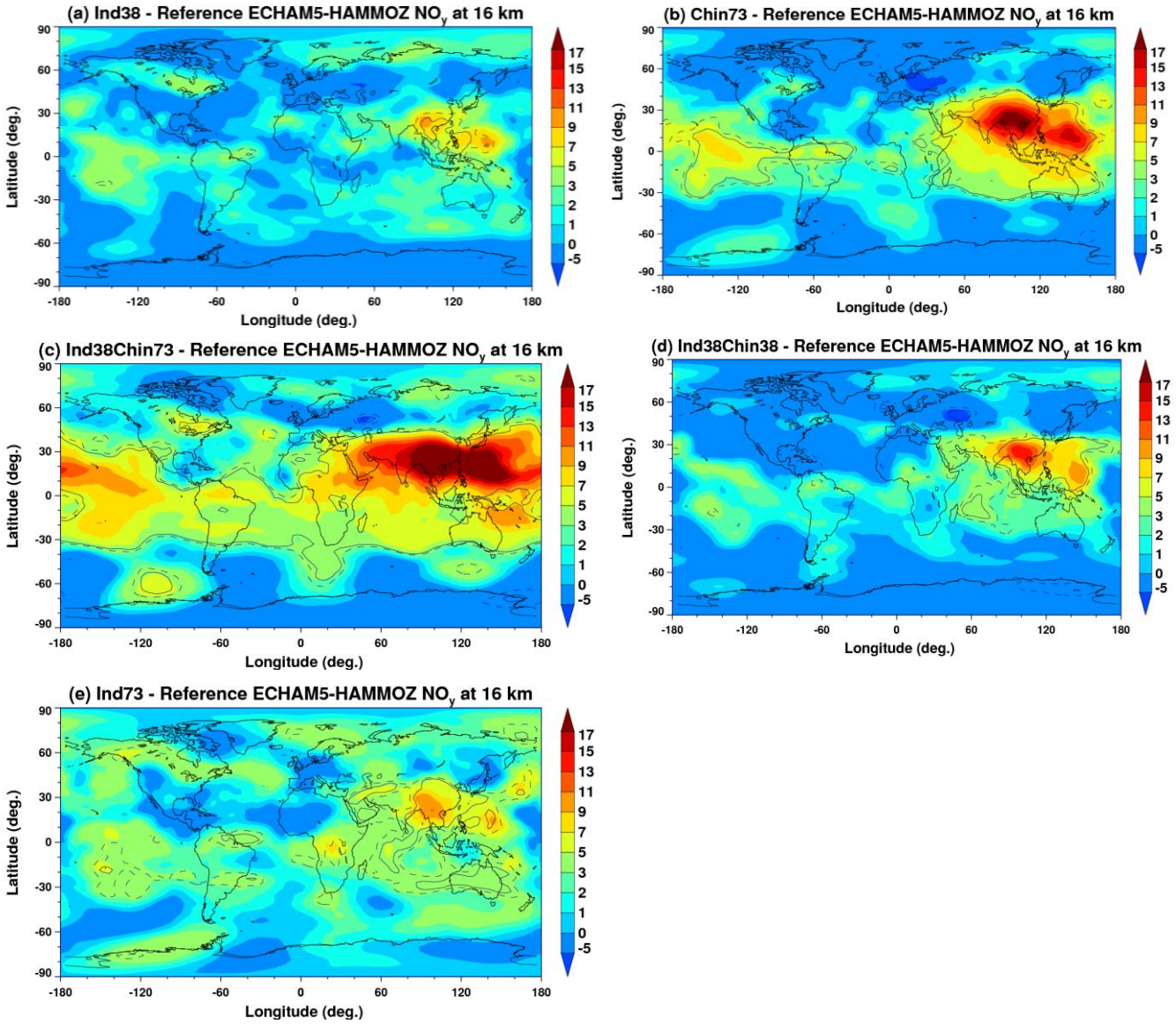

Figure 8 Percentage change in ECHAM5-HAMMOZ NO_Y ($NO+NO_2+NO_3+2*N_2O_5+HNO_3+HNO_4+PAN+MPAN+ONIT+ONITR+ISOPNO_3$) at 16km, as obtained from (a) Ind38 (b) Chin73 (c) Ind38Chin73 (d) Ind38Chin38 and (e) Ind73 simulations. Solid black line indicates the 95% Student's t test confidence interval while dashed line indicates 90% confidence interval.

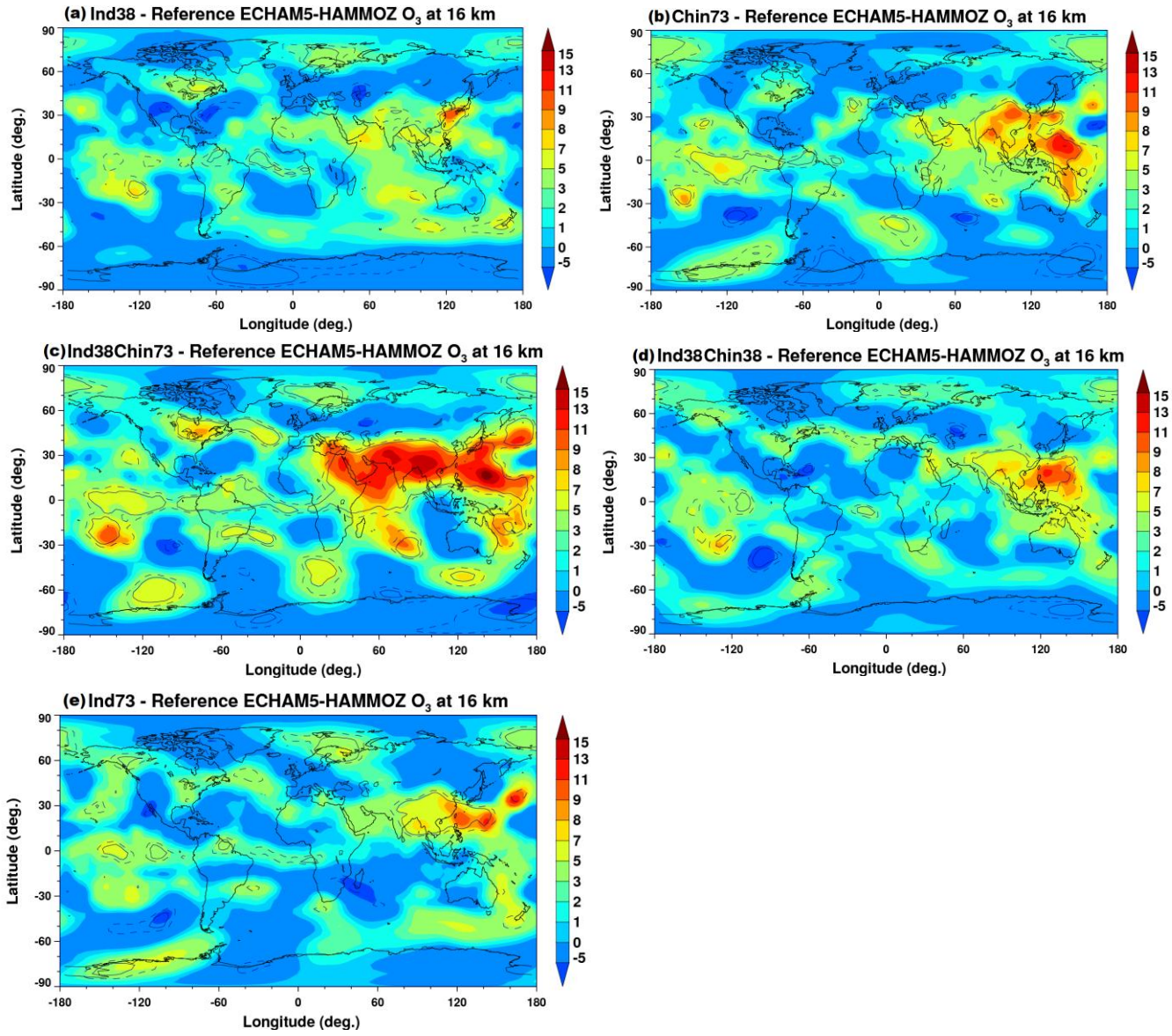

Figure 9 Percentage change in ECHAM5-HAMMOZ ozone at 16km , as obtained from (a) Ind38 (b) Chin73 (c) Ind38Chin73 (d) Ind38Chin38 and (e) Ind73 simulations. Solid black line indicates the 95% Student's t test confidence interval while dashed line indicates 90% confidence interval.